Deadwood

Adrien Peytavie, James Gain, Eric Guérin, Oscar Argudo, Eric Galin

DeadWood

Including disturbance and decay in the depiction of digital nature

ADRIEN PEYTAVIE, Université Lyon 1, CNRS, LIRIS, France
JAMES GAIN, University of Cape Town, South Africa
ERIC GUÉRIN, INSA-Lyon, CNRS, LIRIS, France
OSCAR ARGUDO, Universitat Politècnica de Catalunya, Spain
ERIC GALIN, Université Lyon 1, CNRS, LIRIS, France

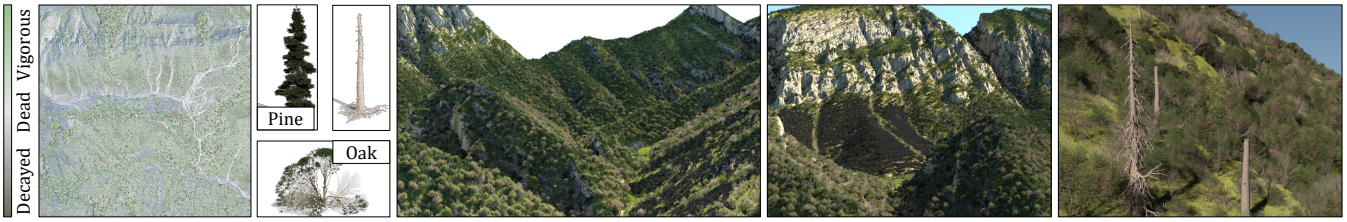

Fig. 1. Our system connects the ecosystem simulation of plant life histories, incorporating disturbance and decay, with a model realization process that instantiates individual trees, resulting in the creation of visually rich natural scenes.

The creation of truly believable simulated natural environments remains an unsolved problem in Computer Graphics. This is, in part, due to a lack of visual variety. In nature, apart from variation due to abiotic and biotic growth factors, a significant role is played by disturbance events, such as fires, windstorms, disease, and death and decay processes, which give rise to both standing dead trees (snags) and downed woody debris (logs). For instance, snags constitute on average 10% of unmanaged forests by basal area, and logs account for $2\frac{1}{2}$ times this quantity.

While previous systems have incorporated individual elements of disturbance (e.g., forest fires) and decay (e.g., the formation of humus), there has been no unifying treatment, perhaps because of the challenge of matching simulation results with generated geometric models.

In this paper, we present a framework that combines an ecosystem simulation, which explicitly incorporates disturbance events and decay processes, with a model realization process, which balances the uniqueness arising from life history with the need for instancing due to memory constraints. We tested our hypothesis concerning the visual impact of disturbance and decay with a two-alternative forced-choice experiment ($n = 116$). Our findings are that the presence of dead wood in various forms, as snags or logs, significantly improves the believability of natural scenes, while, surprisingly, general variation in the number of model instances, with up to 8 models per species, and a focus on disturbance events, does not.

Authors' addresses: Adrien Peytavie, Université Lyon 1, CNRS, LIRIS, France, adrien.peytavie@liris.cnrs.fr; James Gain, University of Cape Town, South Africa, jgain@cs.uct.ac.za; Eric Guérin, INSA-Lyon, CNRS, LIRIS, France, eric.guerin@liris.cnrs.fr; Oscar Argudo, Universitat Politècnica de Catalunya, Spain, oscar.argudo@upc.edu; Eric Galin, Université Lyon 1, CNRS, LIRIS, France, eric.galin@liris.cnrs.fr.

CCS Concepts: • **Computing methodologies** → **Shape modeling**.

Additional Key Words and Phrases: Ecosystem simulation, natural phenomena

ACM Reference Format:
Adrien Peytavie, James Gain, Eric Guérin, Oscar Argudo, and Eric Galin. 2020. DeadWood: Including disturbance and decay in the depiction of digital nature.

1 INTRODUCTION

Without trees, shrubs, forbs and grass, the visual depiction of computer generated natural scenes would be lifeless and dull. Simulated ecosystems (defined to include natural and exclude artificial scene elements) provide an important component in a range of applications, such as computer games, virtual environments, and film. Nevertheless, current solutions fail to fully achieve the rich diversity present in natural environments. Realism goes beyond a surface question of placement, which encompasses the location, species, height and canopy dimensions of plants in a scene, and extends to the events that impact the appearance of individual trees, including evidence of environmental stresses, damage due to disturbance events, and death and decay. Asymmetric growth and regrowth, discoloration, scarring, burns, broken tree limbs, pests, not to mention the presence of snags and logs, all provide crucial direct and indirect visual clues to a viewer as to the characteristics and history of the ecosystem (see Figure 2).

Thus, our key observation is that disturbance events, encompassing wildfires, windstorms, pests and disease, and death and decay processes play a critical part in the realistic depiction of natural scenes. As one example, in unregulated forests, dead and decaying vegetation typically accounts for 30% of the basal area [Nilsson et al. 2002] and is thus visually salient.

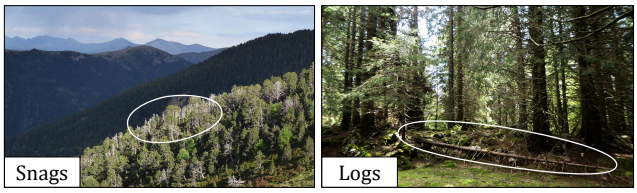

Fig. 2. Snags (standing dead trees) and logs (downed woody debris) often have a significant impact on the appearance of real landscapes.

Fig. 3. Examples of the under-canopy of simulated natural scenes with death and decay represented by snags, fallen branches and logs.

While there are techniques that focus on specific aspects of aging and weathering in computer graphics [Mérillou and Ghazanfarpour 2008], such as rock erosion and fragmentation over time [Dorsey et al. 1999], senescence and decay [Kider et al. 2011] and the organic growth of lichens and mosses [Desbenoit et al. 2004], the unified treatment of disturbance and decay in computer-generated natural scenes has not been adequately addressed. This is likely because it requires retaining a life history of all events impacting a plant's appearance rather than a single final snapshot of state, and also an interdependence between simulation and model realization. Most previous methods focus separately on either plant modelling or ecosystem simulation to the detriment of both. A notable exception is the work of Makowski *et al.* [2019] and its sequels [Palubicki et al. 2022], which represent trees during both simulation and modelling as a collection of branch modules and also account for disturbance by fire [Hädrich et al. 2021] and wind [Pirk et al. 2014]. In contrast, our approach supports larger-scale forests (with millions of trees), provides a separation between simulation and tree geometry instancing, and considers death and decay in detail (see Figure 1).

We achieve these goals (as shown in Figure 3) in three phases. First, we simulate the development of individual trees with the purpose of sampling the range of achievable plant phenotypes from seedlings all the way to rotting stumps so as to support the curation of a database of visually representative geometric models and also to provide allometry data that bounds the size and scaling relationships of plant specimens. This takes place for different species under variable conditions, including differential access to resources depending on weather and terrain scenarios, crowding by competitors ranging from isolated singletons to dense communities, and a suite of disturbance and decay events. Second, we perform an individual-based ecosystem simulation that respects these allometries and incorporates both disturbance events and decay processes. Third, the life-history of the resulting plants is fed to a multi-criteria matching process and the geometry for a set of plant archetypes is derived and placed on the terrain. For small-scale scenes each tree can be unique but for forests of significant size some form of instantiation is required even by modern renderers.

Our key contributions are as follows: (1) an extension of existing growth models [Palubicki et al. 2009] that respects a detailed life history of influencing events and produces, on a yearly basis, both detailed geometry and allometric data, (2) an enhanced ecosystem simulation, building on the work of Kapp *et al.* [2020], that accounts for disturbance events and decay processes, and produces a detailed life and death history for every specimen, (3) a model quantization approach that balances database size and visual saliency, and (4) a decoupling of the growth model and simulation so that final model realization can be deferred to the last phase of the pipeline, while still ensuring that simulated trees are achievable within the growth model. We validate our framework through a two-alternative forced choice (2AFC) perceptual study, which demonstrates that viewers regard natural scenes where decaying wood is present as more believable.

2 RELATED WORK

There is a considerable body of literature attacking the problem of plant modelling and rendering by employing a mix of procedural, simulation, and data-driven strategies, and ranging in scale from individual trees to entire forests (see Figure 4). Our method focuses strongly on the simulation angle at both extremes of scale as a route to visual diversity and realism.

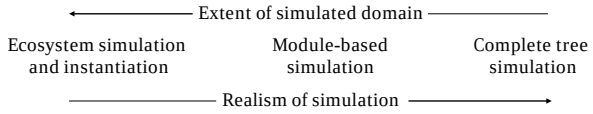

Fig. 4. The spectrum of ecosystem simulation strategies.

Early efforts in modelling individual plants were mostly concerned with issues of procedural generation, but attention soon shifted to context sensitivity as a way to produce more realistic shapes through adaptation to the environment [Benes et al. 2009; Hadrich et al. 2017; Měch and Prusinkiewicz 1996; Prusinkiewicz et al. 2001], as well as sourcing input from sketches [Wither et al. 2009], exemplar components [Maréchal et al. 2010; Xie et al. 2016], images [Bradley et al. 2013], and videos [Li et al. 2011]. More recently, the focus has been on reconstructing botanical trees from single images [Li et al. 2021] and point clouds [Liu et al. 2021].

For individual tree models, an emphasis on simulation has enabled a greater exploration of shape variety. This includes the detailed consideration of fire [Pirk et al. 2017] and wind [Pirk et al. 2014] impact, deformation and pruning that is consistent with obstacles and shade [Pirk et al. 2012b], and reverse-engineering the growth trajectory of a plant leading up to a single provided model [Pirk et al. 2012a].

At the other end of the scale spectrum, the most common approach to generating large-scale ecosystems is to derive an underlying statistical distribution, by observation or analysis, and then synthesize plant positions accordingly. Here, techniques include density-based point patterns [Deussen et al. 1998], probability

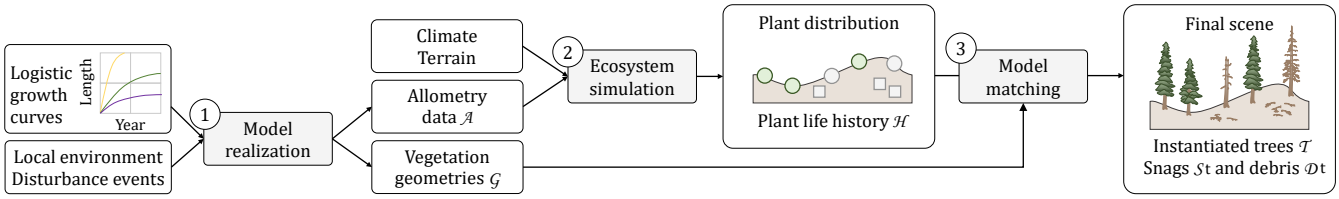

Fig. 5. An overview of ecosystem creation: growth simulations of individual trees (1) are performed based on species growth curves and a range of disturbance events. The resulting data in the form of allometries, along with an environmental scenario that prescribes the climatic and terrain conditions and disturbance events over time, is used for an ecosystem simulation (2). The outcome is fed to a matching instantiation process (3), which takes account of plant life history $\mathcal{H}$ and geometry $\mathcal{G}$ from the growth simulations to realize a final scene.

						Deadwood	Disturbance			
Method	Reference	Snags	Logs	Decay	Humus	Seeding	Fire	Wind	Disease	Fauna
Silviculture	[Makowski et al. 2019]	+					+	+	+	
Eco-erosion	[Cordonnier et al. 2017]	+			+		+	+		
Flora-Fauna	[Ecormier-Nocca et al. 2021]									+
Deadwood		+	+	+		+	+	+	+	

Table 1. A comparison of death, decay and disturbance features among ecosystem simulation frameworks. Columns cover whether the framework portrays snags and logs, simulates their decay, represents the formation of humus, alters the seeding probability of plants depending on the presence of a matrix of deadwood, and captures disturbance events caused by fire, wind, disease and fauna (the impact of humans and animals). The *Siviculture* entry covers the original paper and subsequent work addressing fire [Pirk et al. 2017] and wind [Pirk et al. 2014]. Our *Deadwood* system does not address the formation of humus because this is a very long term process. In addition, we leave disturbance due to human and animal impact as future work.

density maps [Lane and Prusinkiewicz 2002], Wang tiles [Alsweis and Deussen 2006], dart throwing [Andújar et al. 2014], cluster merging [Li et al. 2018], distance-based distribution histograms [Ecormier-Nocca et al. 2019; Gain et al. 2017], and, most recently, machine learning of real-world distribution data [Kapp et al. 2020; Niese et al. 2022; Zhang et al. 2019]. While computationally efficient and hence applicable to large scenes, such approaches do not always simulate the full life history of plants, including death and disturbance processes, and therefore have difficulty in capturing the variability and complexity inherent in real ecosystems.

To achieve a faithful depiction of nature a full ecosystem simulation that accounts for seeding, growth subject to resource competition and disturbance effects, and eventual death and decay is arguably the best approach. Unfortunately, this increase in fidelity comes at the expense of efficiency, with simulations usually running to minutes or hours, depending on the scale of the scene and the level of abstraction inherent in the simulation model. With regard to the latter, it is typical to use abstraction based on radial interactions [Alsweis and Deussen 2005; Deussen et al. 1998; Gain et al. 2017; Kapp et al. 2020], L-systems [Lane and Prusinkiewicz 2002], agents [Bradbury et al. 2015; Ch'Ng 2013; Ecormier-Nocca et al. 2021] or branch modules [Makowski et al. 2019; Palubicki et al. 2022].

The most common mechanism for handling mortality in simulations is to simply remove the individual plant from the simulation at the instant of death. Unfortunately, this ignores the significant part that dead and decaying plants play in an ecosystem. Cordonnier *et al.* [2017] is among the works that explicitly consider decay. However, this is cast in terms of the connection between the overlying ecosystem and the underlying terrain, specifically the conversion of dead plant matter into soil humus, rather than the visual evolution embodied in the decay process. The Sylviculture framework [Makowski et al. 2019; Palubicki et al. 2022] comes closest to matching our overarching goals in that it links ecosystem simulation to model realization through a branch module abstraction. In contrast, we achieve both greater abstraction during ecosystem simulation and more options during instantiation by using plant allometries and life history, which afford a less restrictive coupling between stages. We also elevate death and decay processes to a more central rôle than previous work. Table 1 provides a side-by-side comparison of the death, decay, and disturbance features of state-of-the-art ecosystem simulation frameworks.

3 OVERVIEW

Our framework for creating natural scenes with per-specimen life histories and the attendant emergent variation has three main stages (see Figure 5):

(1) *Individual Model Realization* - First, we perform a wide variety of structural growth simulations for individual trees (Section 4). These are designed to sample the variation in species, environmental growth conditions, and disturbance events (including wind, disease, and fire) for two reasons: a) to build an atlas of reference geometry for later use during instantiation, and b) to derive statistics of the shape relationships within individual plant specimens (allometries).
(2) *Enhanced Ecosystem Simulation* - Next a large-scale ecosystem simulation (Section 5) is performed. In addition to the normal processes of seeding, growth, and death, this is enhanced to account for disturbance events and decay processes

at both the snag and log level. The end result is a full life-history for every specimen in the resulting ecosystem.

(3) *Instantiation Matching* - Finally, a matching step (Section 6) is used to map the life histories of plants to entries in the reference atlas. This provides a set of model instances for populating the resulting scene. If required, for instance where a subset of the scene has special significance, additional unique models can be generated on demand. Furthermore, it is possible to swap between precomputed atlases depending on the desired balance between memory demands and model uniqueness.

This component structure is aimed at ensuring a form of bijective mapping between simulation and model realization, specifically that the full range of life-histories can be portrayed while at the same time clamping the simulation to the bounds of realizable geometry. Unfortunately, while it may at first seem that the hand off from simulation to model instantiation can be achieved through a simple pass-forward process, it is actually fraught with potential complications. Chief of these is the potential for a mismatch between simulation and instantiation, in which the simulation provides models that are not achievable within the model realization framework, being too broad or tall, or too heavily or sparsely branched, or some combination of these and other factors.

This is further complicated by the nature of our simulation, which employs a relatively abstract individual-based model, representing trees as discs for the purpose of abiotic competition. This means that, while characteristics, such as height and canopy extent are immediately available, other necessary attributes, such as diameter at breast height and number of primary branches, are not intrinsically part of the simulation and must be derived.

Fortunately, the biological and botanical literature provide a single solution to both these problems in the form of allometries [Henry et al. 2013; Sato et al. 2007; Sitch et al. 2008]. These specify characteristic scaling relationships between attributes of living organisms. For instance, for most tree species, in the absence of disturbance events, there is a roughly linear relationship between increases in tree height and canopy extent [Pretzsch et al. 2015]. In our case, during simulation, given the height of a tree of a particular species, we need to derive canopy radius, diameter at breast height, and the number of primary branches (and their average diameter). However, this is further complicated by the species-specific response of trees to local competition for sunlight [Purves et al. 2007]. In dense forests trees tend to grow tall and narrow as they reach for the sun. In contrast in sparser, more isolated communities they are free to allocate resources to spreading outwards rather than upwards.

To solve this we create an envelope of allometries per species (s), as a function of tree age (t) and bounded by the extremes of surrounding tree density (maximum density or isolation). Thus:

$$\mathcal{A}_d(s,t), \mathcal{A}_i(s,t) = \{h, r, \phi, p, \psi\}, \tag{1}$$

where the dense ($\mathcal{A}_d$) and isolated ($\mathcal{A}_i$) allometry functions for a given species and age return a tuple of height (h), canopy radius (r), diameter at breast height (ϕ), number of primary branches (p), and average primary branch diameter (ψ). To derive these functions we perform a geometric growth simulation, as described in Section 4 for each species and case (dense or isolated). By measuring aspects of the resulting individual tree geometry we are able to derive all the required attributes (h, r, ϕ, p, ψ), which can be bundled together into a set of allometry curves.

One difficulty is that even though the allometries are consistent at a given age, since the tree models are a visual match to real-world appearance by design, the growth rate is not, with trees being taller or shorter than expected for their age. To fix this we resample the allometries to fit to an idealized logistic height growth curve widely used in the botanical literature [Tsoularis and Wallace 2002]:

$$h(t) = \left(\frac{2}{1 + e^{(t/\hat{\ell}_s)\, q}} - 1 \right) \hat{h}_s, \tag{2}$$

where $\hat{\ell}_s$ is the maximum achievable tree age, $\hat{h}_s$ is the maximum achievable tree height (which varies according to surrounding tree density), and q is a tuning parameter that allows a better fit to measured real-world height values. Note that these quantities are all species specific (see Table 5 for values). The resulting allometries are central to both our enhanced simulation, establishing growth limits and allowing derivation of secondary attributes, and model realization, ensuring that the features of simulated trees match exactly with corresponding geometric models.

4 MODEL REALIZATION

We require a method for individual plant generation that provides both allometry statistics for the full ecosystem simulation and geometry for model instantiation. This needs to account for a plant's life history, encompassing decay processes, disturbance events, and the biotic and abiotic factors influencing growth. To achieve this we build on the self-organising tree model of Palubicki *et al.* [2009]. The original system is biologically inspired with buds and branches competing for light and space as regulated by internal signalling. The overall tree structure is thus an emergent property. We enhance this model in several ways. First, we adapt the growth rate under ideal conditions so that yearly height increments follow a per-species logistic growth curve derived from the Botany literature [Tsoularis and Wallace 2002]. This allows an alignment between growth in both the model realization and enhanced simulation components (see Figure 6). Second, we improve the evaluation of self-shadowing by casting visibility rays onto a randomly sub-sampled half sphere. The proportion of direct intersection with existing leaves provides a measure of self-shadowing that affects the probability of generating new branches at nodes and accounts for gap dynamics. Third, we add state indicators to branches to support death, decay, and destruction depending on vigor and disturbance.

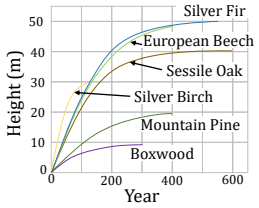

Fig. 6. Logistic height growth curves for different tree species.

4.1 Branch Death and Decay

Our model realization needs to visually portray a gradual process of death and decay. Fortunately, botany already categorises decay into classes for the purpose of forest inventory largely on the basis of

Class	Snag Detail	Log Detail	Density
(1) Intact	Starts fully intact with leaves; gradually loses leaves, twigs and secondary branches	Bark intact, still green	$0.9 - 1.0$
(2) Bare	No leaves or twigs and few secondary branches; gradually loses primary branches	Bark intact, with some side branches	$0.7 - 0.9$
(3) Debranched	Stumps and broken primary branches remain, still full tree height	Patchy bark, no twigs, still round	$0.5 - 0.7$
(4) Snapped | Oval	Main trunk reduced in height	Last traces of bark, oval cross section	$0.3 - 0.5$
(5) Stump | Collapsed	Less than 2 m of trunk remaining	No bark, powdery texture	$0.0 - 0.3$

Table 2. Details of decay classes, including the appearance for both snags and logs and the wood density range occupied.

appearance. Although, there are competing classification schemes we have chosen an approach that both emphasises visual distinctions and allows a transition from snags to logs (see Figure 9 and Table 2). We pair the snag classification of Aakala *et al.* [2008] with the log classification of the U.S. National Forest Inventory [Woodall and Monleon 2008]. These two classifications align so that, for example, a class 3 snag that is uprooted by a windstorm disturbance event will transition to a class 3 log. The main differences lie in the last two stages, where snags are truncated, while logs take on an ellipsoidal cross-section due to vertical collapse [Fraver et al. 2013].

It is common to measure decay quantitatively [Zell et al. 2009] through either density or mass loss, where 1 represents the moment of death and 0 represents total decay. For our purposes average density d_i for a specimen snag or log is simpler and more useful than total mass because it can be tracked for standing trees even when branches fall away and become logs, which would otherwise represent a sudden discontinuous loss of mass. The transitions between decay classes occur at specific values of d_i as per Table 2.

Apart from tree death in its entirety and the resulting transition from live tree to snag, we also model death at the level of individual branches (and their dependent sub-branches). This can be triggered by a lack of resources, tracked using a vigor score v_i, or disturbance, by wind, fire and disease. Such branches cease growing, are subject to decay and fall to form logs, either over time or immediately, depending on the root cause of death. In this case, we parametrize the rate of decay Δd_i according to branch diameter ψ so as to support differential degradation in different subparts of the tree.

4.2 Disturbance Events

It is possible to perform an in-depth simulation of the impact of disturbance events, such as wind storms and forest fires [Pirk et al. 2017], on individual trees. Such simulations involve a complex combination of extrinsic factors (such as wind force and fire intensity and their directions as influenced by the terrain) and intrinsic factors (such as rooting depth, tree health and species-specific resistances). Instead, for simplicity and computational efficiency, we take a phenomenological approach during model realization. A given disturbance event is gradiated from 0 (no effect) to 1 (complete destruction), with gradual random and increasing damage in-between (see Figure 14). For instance, in the case of increasing wind force more and larger branches are either partially broken and left hanging, or completely detached and scattered on the ground in accordance with wind direction and slope. In the most extreme cases, the entire trunk is split or uprooted. Fire on the other hand, involves iterative destruction and blackening in order of ascending branch diameter.

In summary, our model realization component employs a self-organising model of individual plant growth that explicitly incorporates decay classes for snags, logs, and sub-parts of living trees, and also takes a phenomenological approach to modelling disturbance events from sources such as wind storms and forest fires.

5 ENHANCED SIMULATION

The choice of level of abstraction is one of the main differentiators between ecosystem simulation models. This can be as broad as global vegetation models, where the resolution of measurement spans kilometers and species are grouped into plant functional types, or as fine as individual-based models that capture internal processes, such as photosynthesis and transpiration.

Our choice is to adapt a relatively abstract individual-based model [Cordonnier et al. 2017; Gain et al. 2017; Kapp et al. 2020] that represents tree canopy and root systems using discs for the purpose of competition for light and moisture. We enhance this framework to explicitly account for decay at the level of standing dead trees (snags) and downed woody debris (branches) and disturbance events, such as disease, fire, and wind storms. During simulation we store a life history of physical attributes, denoted as $\mathcal{H}$, including height, canopy radius, vigor, disturbance impact, and decay as a tuple per timestep for each plant. This enables later geometric instantiation of individual trees at a chosen level of detail during model realization. This separation between simulation and model realization is motivated primarily by memory and computational efficiency considerations. It stands in contrast to a branch-module strategy [Hädrich et al. 2021; Makowski et al. 2019; Palubicki et al. 2022], which uses tree geometry during simulation, albeit using an abstraction of secondary branches and their subsidiaries that supports GPU instancing.

5.1 Core processes

Our ecosystem simulation extends the individual-based model of Kapp *et al.* [2020] beyond the understorey domain and to include

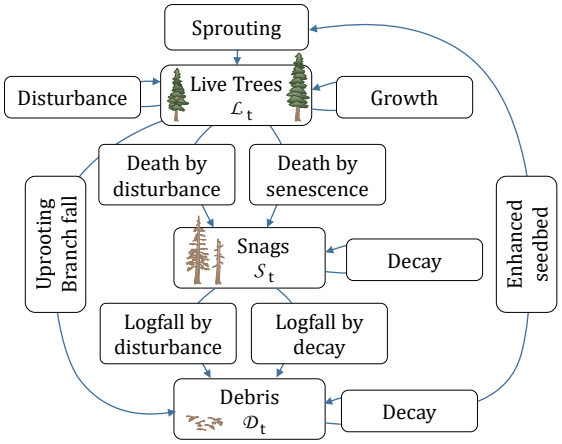

Fig. 7. An overview of enhanced tree simulation. Trees sprout and then grow while being influenced by disturbance events. They may die due to old age, stress or disturbance, and transition to snags. At the same time, logs falling from trees both alive and dead create debris. Snags and logs are subject to decay, with decaying logs providing fertile ground for seed germination.

disturbance and decay processes. We provide here a terse introduction to the original model, sufficient to highlight important notation and indicate where changes are necessary.

We discretize the landscape into a coarse grid (at 1−3m resolution) for the purposes of capturing abiotic factors, such as elevation (from which slope m and temperature τ are derived), sun exposure e, and soil moisture w, as per Cordonnier *et al.* [2017] and Gain *et al.* [2017]. This is overlaid by a fine sub-cell grid (typically at 20 – 30 cm resolution) in order to handle direct competition between plants for access to sunlight and water.

Individual plant vigor is assessed on a monthly basis (the simulation timestep is 1 month) and contributes to a carbon pool that is used, in the case of abundance, to spur growth or, in the case of depletion, to model stress and eventually death. Death, decay and germination processes are considered on a once-yearly basis.

We turn now to a more detailed discussion of the core processes of growth, germination, and death as shown in Figure 7. (Note that in the presentation that follows subscript i denotes individual plants, while subscript s is reserved for specific species).

Growth: In our model the roots and canopies of trees are represented as discs sorted according to relative height. Access to sunlight and moisture is then averaged over the sub-cells intersected by these discs. For sunlight, the received value is attenuated according to species-specific leaf transparency in tallest to shortest order within a sub-cell. For moisture, a defined minimum is allocated starting with the deepest root system, and any excess is shared equally with a single share set aside for seeding. Other abiotic factors, such as slope and temperature, are accessed directly and not attenuated. The vigor of a plant $v_i(\mathbf{p})$ in cell position $\mathbf{p}$ is calculated as a minimum over the contributing abiotic factors, according to Kapp *et al.* [2020]:

$$v_i(\mathbf{p}) = \min(f_\tau \circ \tau(\mathbf{p}), f_w \circ \widetilde{w}(\mathbf{p}), f_e \circ \widetilde{e}(\mathbf{p}), f_m \circ m(\mathbf{p})), \tag{3}$$

where $\widetilde{w}$ and $\widetilde{e}$ are moisture and sunlight exposure subject to local competition, and f_τ, f_m, f_e and $f_w \in [-a, 1]$ are plateaued smooth adaptation functions taking the form $f = g \circ d$, with:

$$g(d) = (1 + a)\, e^{(d/r_s)^{4.5} \ln(0.2)} - a, \qquad d(x) = |x - c_s|. \tag{4}$$

Here, a encodes the maximal stress value (we typically use $a = 0.2$) achieved at and beyond an abiotic distance r_s from the ideal c_s. The parameters c_s and r_s are tuned for each species (see Table 5).

Subsequently, this vigor value is added to the current carbon pool $\mathcal{R}_i$ for the tree. The carbon pool has a unit capacity implying that a plant with optimal reserves can survive $1/a = 5$ months of maximum damage before becoming stressed. If the carbon pool overflows during the growing season then the excess $o_i = \mathcal{R}_i - 3a$ contributes to growth. Conversely, if the carbon pool becomes negative then this factors into potential mortality.

During the months of its growing season the idealized age of the specimen is advanced in proportion o_i. This is idealized in the sense that it does not track calendar age but rather the cumulative growth relative to the ideal. This allows changing circumstances to result in spurts or retardation of growth. Finally, from the current idealized age and its increment and the relative density of surrounding trees we obtain the change in tree height (h), canopy radius (r), diameter at breast height (ϕ), and primary branch attributes using the allometry functions ($\mathcal{A}_d(s,t)$, $\mathcal{A}_i(s,t)$) derived during model realization. Note that vigor calculations are still performed at monthly intervals outside of the growing season in order to track the state of the carbon pool and its natural depletion during winter months.

Germination: The dispersion of seeds is not modeled explicitly in our system. Rather, for the sake of efficiency we adopt a seedbank approach. On a yearly basis, every cell in our simulation grid not already containing a trunk is tested for potential seedling establishment with one of two germination probabilities γ_{logs} or γ_{bare}, depending on the presence or absence of decaying logs, which act to shelter and promote plant establishment.

After passing this test we still need to account for site suitability. So, for the previous growing season, at a particular sub-cell location $\mathbf{p}$, the sunlight that reaches the forest floor after filtering by canopies and the moisture remaining after allocation to roots is used to calculate the vigor $\overline{v}_s(\mathbf{p})$ of each candidate species. Germination is allowed to proceed with probability equal to $\max_s(\overline{v}_s(\mathbf{p}))$, ensuring that resource-starved sites are not overpopulated.

Finally, if germination is confirmed, a particular species is allocated using roulette wheel selection based per species on the following probability [Kapp et al. 2020]:

$$w_s = \max(\alpha_s \cdot \overline{v}_s(\mathbf{p}) / \hat{\ell}_s^{\beta}, 0), \tag{5}$$

where $\hat{\ell}_s$ is the species-specific maximum expected lifespan, β is an exponent establishing a balance between short- and long-lived plants, and α_s is a multiplier based on the propensity of a species to root in decay-rich soil. We have found, in practice, that $\beta = 1.2$ adequately reflects the higher proportion of seeds generated by short-lived plants, which reach seeding maturity more rapidly.

Death: For efficiency reasons, we check for plant mortality on a yearly rather than monthly basis. Each plant is tested against a death probability $\mu \in [0, 1]$ that combines terms for background mortality

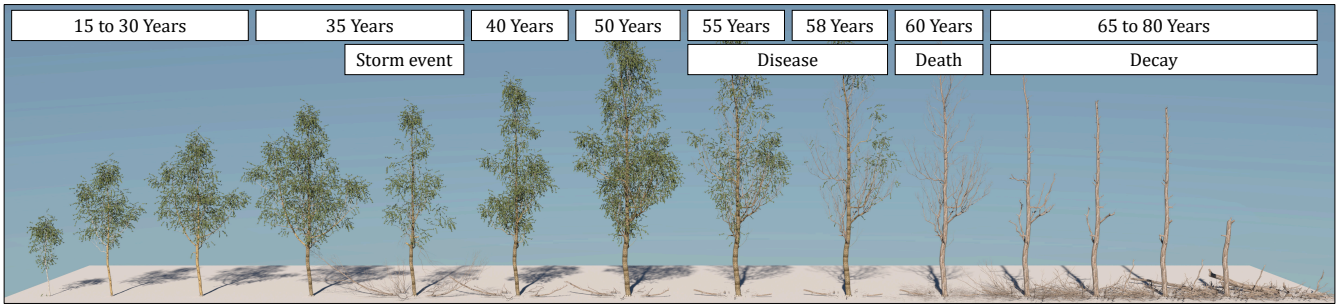

Fig. 8. A typical sequence of tree models generated by our model realization process over a life history that includes disturbance events, death, and decay.

(controlling for species-specific lifespan) and stress-induced mortality (factoring in poor growth conditions and disturbance), where:

$$\mu = \min(\mu_b + \mu_s, 1), \tag{6}$$

$$\mu_b = 1 - \hat{p}^{1/\hat{\ell}_s}, \tag{7}$$

$$\mu_r = \max(-\mathcal{R}_i, 0). \tag{8}$$

The background term μ_b with $\hat{p} = 0.01$ employs discrete survival statistics to enable an expected proportion of 1% of the species to survive under reasonable conditions to a maximum age $\hat{\ell}_s$. The stress term μ_r is based on the extent to which the carbon pool is overdrawn during the course of the year as a result of resource access, competition and disturbance. Once a tree dies it transitions to the decay cycle (see Figures 8 and 9).

Key changes to the core algorithm are: the revised treatment of allometries, the inclusion of decay-rich germination terms (γ_{log} and α_s), and the impact of disturbance on the carbon pool $\mathcal{R}$ and hence stress-based mortality μ_r. These and other changes will be motivated and explained more fully in subsequent sections.

5.2 Decay

As is natural, our treatment of decay mirrors that of growth. They are both biological processes that take place over time and are subject to particular biotic and abiotic influences. A distinction is made between trees that die but remain rooted and upright, known as standing dead wood or snags, and trunks and branches that have fallen, known as downed woody debris or logs. From a simulation perspective, both categories undergo similar decay processes, albeit accelerated in the case of logs. Broadly speaking, our decay simulation proceeds as follows: at the moment of death we calculate the expected duration of decay (the *deathspan*) factoring in the species and diameter of the snag or log. Then on a yearly basis we increment the nominal time since death while adjusting for moisture and temperature conditions. Instead of measuring decay directly, we use wood density ($d_i \in [1, 0]$) as a proxy, which is linked to nominal aging through a sigmoidal function. For model realization, we borrow the common botanical practice of separating the continuum of decay into classes for both snags and logs [Russell et al. 2015]. These represent visually distinct stages, as illustrated in Figure 9, and evidenced in renderings of trees models instantiated from the geometry database in Figure 10.

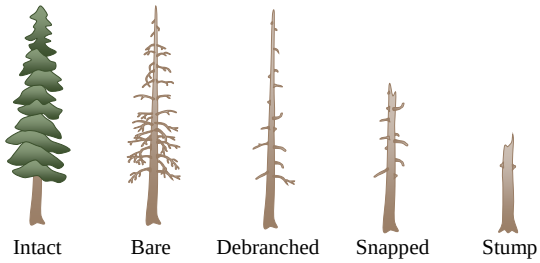

Fig. 9. The five decay stages following tree death used to classify standing dead trees (snags).

We turn now to a detailed motivation and explanation of this decay process. It is necessary to account for moisture, temperature, species, and initial wood volume to properly model the decay process with any accuracy [Zell et al. 2009]. Since decay is largely a biological process involving micro-organisms and invertebrates there are optimal conditions in terms of temperature and moisture for these entities to thrive. For example, the effects of moisture are often modeled as a quadratic function [Zell et al. 2009] with an overabundance or scarcity of moisture both retarding decay. Furthermore, the particular species and its wood characteristics (such as density, bark thickness and retardant chemistry) are known to have a significant impact. Finally, the initial biomass must also be accounted for. Since organisms initially attack the exterior, a larger diameter, and hence higher volume to surface area ratio, means that decay will take longer.

We thus use the following inputs to model decay as a once-yearly process: yearly mean temperature $\overline{\tau}(\mathbf{p})$ at site $\mathbf{p}$, accounting for altitude and shifting weather patterns; yearly mean moisture $\overline{w}(\mathbf{p})$ arriving at location $\mathbf{p}$, prior to absorption and use by neighboring plants; maximum trunk or log diameter (ϕ), which is derived by allometry, and species s. Certain biotic quantities (such as height and trunk diameter) are frozen at the moment of tree death or log fall and so can be used to calculate the deathspan at the start of the decay simulation:

$$\delta_i = \alpha_\phi \cdot \phi_i \cdot \hat{\delta}_s, \tag{9}$$

where $\hat{\delta}_s$ is the fastest time to complete decay for a tree of species s with a diameter of 10 cm, and α_ϕ weights the impact of the diameter on the deathspan.

Fig. 10. A small forest scene with trees at different decay stages.

Then on a yearly basis, the nominal time since death is incremented. However, this still needs to account for the change in yearly abiotic conditions. We calibrate δ_i to represent the deathspan subject to maximal decay and retard this process when conditions are suboptimal from a fungal, microbial, and invertebrate perspective. To model this the time increment is adjusted according to a minimum of viabilities function as was done for plant vigor:

$$\Delta t = \min(f_\tau \circ \overline{\tau}, f_w \circ \overline{w}). \tag{10}$$

The difference here is that the viability function has a range in [0,1] (i.e., $a = 0$) and the viabilities are not species specific. Of course, the particular micro-organisms that cause decay in different plants do vary, and with them the impact of abiotic factors, so this is only an approximation.

Finally, we need to record the density of the decaying snag or log since it is this metric, and its correlation with decay class [Russell et al. 2015], that is used by model realization. Density is set to 1 at the moment of death and reaches 0 at the end of the deathspan. In terms of density loss over time, the are several choices of function [Russell et al. 2015; Zell et al. 2009], including linear, exponential, piecewise, and sigmoidal. While exponential functions are most common, possibly due to their applicability in regression, we adopt a sigmoid function, which is thought to provide a better fit [Freschet et al. 2012], because the decay process generally begins slowly at first before speeding up, with a gradual slowdown at the end.

Thus, we choose a sigmoidal function (using smoothstep $s(x) = (-2x^3 + 3x^3), x \in [0, 1]$ due to its invertibility) that relates time since death for a snag or log ($t_i \in [0, \delta_i]$) to its density ($d_i \in [1, 0]$):

$$d_i = s(t/\delta_i) \tag{11}$$

It may seem that using set values for decay class transition neglects the impact of abiotic and biotic factors, but these are accounted for in the time step processes of Equations 9 and 10. Note that our choice of a once-yearly decay evaluation may introduce some bias in cases where average moisture and temperature do not capture highly variable weather, but we regard this as an acceptable tradeoff for efficiency, given that such an averaging approach accounts for about 80% of the variance in decay [Zell et al. 2009].

5.3 Disturbance events

While abiotic stressors and senescence factors play a part in the damage and ultimate death of trees, disturbance events, such as wind, snow, frost, fire, drought, landslides, flooding, animal grazing and human intervention [Gardiner and Quine 2000], are of equal importance in shaping an ecosystem.

Within our system, we incorporate different forms of disturbance as external modules (see Figures 12, 11, and 13). These impact the state of the ecosystem based on disturbance events that are either scripted according to a timeline scenario or triggered based on a stochastic distribution. As a demonstration of this mechanism we have implemented four classes of disturbance, with varied duration, locality, and species impact, namely: wildfires, wind storms, diseases, and droughts.

Fig. 11. Impact of a wind storm event: trees are uprooted, and branches are fractured and broken.

5.3.1 Wildfires. Our philosophy of coupling course-grained simulation with fine-grained model instantiation applies equally well to the case of modelling forest fires. On the simulation side, we build on an extant grid-based Cellular Automata (CA) model [Alexandridis et al. 2008], which aligns well with the existing discretization of abiotic influences and growth processes.

Within the CA grid, each cell can take on one of four states: non-flammable, un-ignited, burning, or burnt. Initially, fire is seeded at one or more locations and cells within a threshold distance are marked as burning. Then, propagation rules are iteratively applied until no burning cells remain. First, burning cells transition to burnt after a single iteration. Second, on each iteration burning cells propagate to un-ignited 8-way neighbors, according to the following burn probability:

$$P_{\text{burn}} = P_0\,(1 + P_{\text{veg}})\,(1 + P_{\text{den}})\,P_{\text{b}}\,P_{\text{m}}\,P_{\text{w}}\,P_{\text{h}}. \tag{12}$$

P_0 represents the baseline probability of fire propagating over flat terrain in the absence of wind; $P_{\text{veg}}, P_{\text{den}} \in [-1, 1]$ account for the type and density of vegetation in a cell, respectively; P_{b} models the effect of wind speed V and the angle θ_b between wind direction and fire propagation; P_{m} captures the influence of slope angle m, since fire propagates more aggressively up steep slopes; P_{w} factors in the impact of moisture percentage C_w on the spread rate, and $P_{\text{h}} = h^d$ models how crown height affects fire spread. Specifically,

$$P_{\text{b}} = e^{V(c_1 + c_2(\cos\theta_b - 1))} \quad P_{\text{s}} = e^{am} \quad P_{\text{w}} = a\,e^{-bC_w}, \tag{13}$$

where c_1, c_2, a, b and d are tuning parameters [Alexandridis et al. 2008].

We turn to the simulation grid to derive quantities needed for the burn probability P_{burn}. Vegetation density for P_{den} is estimated per cell from the volume of incident trunks, canopies, snags and logs

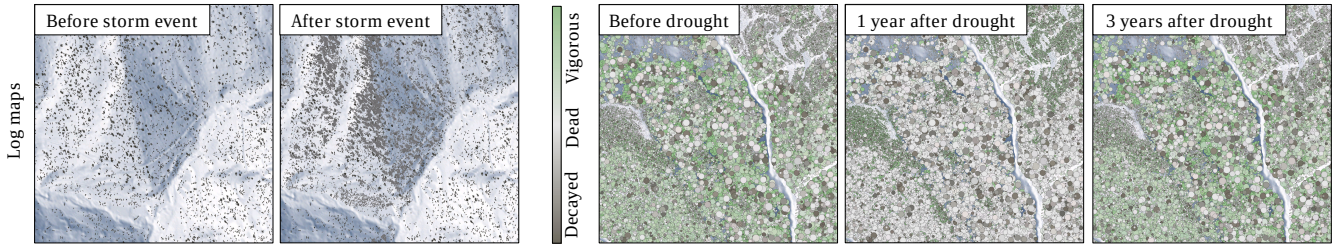

Fig. 12. The impact of disturbance events on ecosystem state. (Left) In a mature undisturbed forest logs are evenly distributed, but exhibit clustering in the path of a windstorm. (Right) Severe short-term drought suppresses plant vigor, but recovery is rapid once rainfall normalizes.

moderated by density reduction due to decay. The moisture content C_w is derived from the viability (carbon reserves) and decay for live and dead trees, respectively. Finally, canopy height h is the height of the tallest specimen in a cell, or zero if empty.

Once the propagation simulation is complete, we derive a fire damage value $\mathcal{F}(\mathbf{p})$ at a location $\mathbf{p}$ by bilinearly interpolating the binary burnt-unburnt mask. This damage is applied to live trees by proportionally reducing plant reserves (leading to stress and potential death) and to snags and logs by proportionally advancing decay. In all cases, the fire event and damage value $\mathcal{F}(\mathbf{p})$ are recorded in a specimen's life history $\mathcal{H}$ for use in model realization.

The CA model does not explicitly associate a duration with its iterations, so a wildfire is implicitly contained within a single month. However, it would be possible to implement a multi-month wildfire by limiting the number of CA propagation steps in a simulation month, and resuming it on the next.

5.3.2 Wind storms. Powerful storms can radically alter a forested landscape through widespread snapping of branches and trunks, as well as uprooting. To incorporate this form of disturbance we follow Seidl *et al.* [2014] and compute the critical wind speeds for uprooting, and trunk and branch snapping (w_u, w_s and w_b, respectively) for trees in the path of a storm:

$$w_u = \left(\frac{C_s \cdot GW_i}{\kappa_i}\right)^{1/2} \qquad w_s = \left(\frac{MOR_s \cdot \phi_i^3 \cdot \pi}{32 \cdot \kappa_i}\right)^{1/2}, \tag{14}$$

and $w_b = 65\,\text{km/h}$ in accordance with the Beaufort wind scale. In these equations, C_s is a per-species coefficient obtained from pulling experiments, MOR_s is the species modulus of rupture, GW_i is the green stem weight, and κ_i is the specimen's turning moment coefficient as a function of height and diameter [Hale et al. 2015]:

$$\kappa_i = 111.7 \cdot \phi_i^2 \cdot h \tag{15}$$

To derive green stem weight, we multiply the approximate volume of the tree by the wood density of the species (ρ):

$$GW_i = \rho \cdot f_w \cdot V = \rho \cdot f_w \cdot \frac{\pi}{4} \phi_i^2 h_i f_V. \tag{16}$$

In this approximation, f_w is the wet biomass factor (set to 1 for snags and 1.85 for live trees) and f_V is a per-species volume form factor. Seidl *et al.* [2014] incorporate additional dimensionless coefficients in their formulation to account for wind shadow effects, where trees are shielded from the wind by the mass of a forest or terrain topography. Instead, we use the terrain heightfield and canopy heights to compute a directional occlusion map relative to the wind direction, using a strategy similar to Screen Space Directional Occlusion [Ritschel et al. 2009]. To obtain a per tree wind force w_i we scale the maximum wind speed of the storm according to this occlusion.

Finally, tree damage can be determined: if $w_i > w_u$ or $w_i > w_s$, the tree will either uproot or snap. Otherwise, for wind speeds in the range $w_b < w_i < \min(w_u, w_s)$ we apply a linearly increasing probability of breaking primary branches. When a specimen suffers damage due to a wind storm, we record a wind event together with the damage type (branch, uproot, or snap) in its life history $\mathcal{H}$.

5.3.3 Disease. There are a plethora of pathogens that can affect the health of a tree, ranging in scale from bacteria to fungi and variously impacting specific species and tree components (such as leaves, roots and stems). Take, for instance, the case of dutch-elm disease, which is a species-specific fungal infection that has destroyed half of the elms in Europe and three-quarters of those in North America.

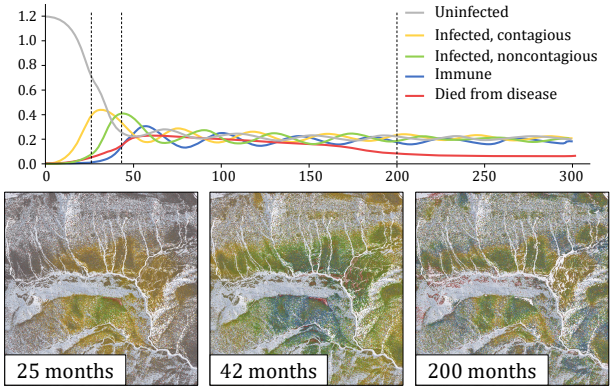

Fig. 13. Disease progression: (above) a graph showing the number of trees (in millions) for different disease classes over a period of 300 months, and (below) snapshots of the corresponding ecosystems at the 25, 42, and 200 month marks. The progression shows a typical surge in initial infection and death, with subsequent waves that gradually damp down to an endemic state.

To include this important source of disturbance we adopt the Susceptible-Infected-Recovered (SIR) framework used for contagious diseases [Bjørnstad et al. 2020; Tolles and Luong 2020]. Our

implementation is relatively straightforward: individuals of the target species for a disease are marked as *susceptible*, then a random subsample are shifted to *infected* and act as a starting vector for the disease. Over an initial contagious period of $m_{\text{contagious}}$ months an infected individual spreads the disease to adjacent susceptible individuals within radius r_{spread} according to a transmission probability P_{spread}. During each month of infection an infected specimen has its carbon pool reduced by a constant $-v_{\text{disease}}$, with the resulting stress possibly leading to death. If a plant survives for m_{recover} months it is classified as *recovered*, with permanent infection achieved by setting $m_{\text{recover}} = \infty$. Recovered plants can acquire temporary or permanent immunity to the disease, according to the value of the parameter m_{immune}. The specimen's history $\mathcal{H}$ records the infection and recovery timestamps.

In our implementation, several diseases can coexist even within the same target species. At every monthly step of the simulation and for each active disease, susceptible individuals query their infected neighbors $\mathcal{N}_i$ within r_{spread} distance and test a random draw against an infection probability $P_i = P_{\text{spread}}\, s(d_i)$, where $s(x)$ is the smoothstep function and d_i the density of infected neighbors:

$$d_i = \frac{1}{\pi r_{\text{spread}}^2} \sum_{j \in \mathcal{N}_i} \pi r_j^2$$

Despite its simplicity, this approach is sufficient to broadly model many species-specific infectious plant diseases and their impact on weaker individuals.

5.3.4 Drought. Changes in the yearly rainfall patterns, which can indirectly affect the vigour of many plant species, are specified in our simulation by a starting month and year, followed by a sequence of n fractional values $d_1, \ldots, d_n$ for a drought duration of n months. During this period, we scale the corresponding monthly precipitation rates by d_i and recompute the moisture map. The reduced moisture available in the simulation cells increases the competition for resources between neighboring plants, leading to a reduction in their viability and carbon pool reserves and an increase in their stress, which occasionally causes the death of some specimens, particularly if the drought is sustained.

6 MATCHING

While it is possible in smaller scenes to generate unique geometry that accurately captures the specific development of each and every tree, this is not achievable from a memory and computation standpoint for larger scenes containing more than a few thousand trees. Instead, we apply an instancing and quantization strategy that dates back to the earliest days of ecosystem rendering [Deussen et al. 1998]. Effectively, we select samples in the biotic and abiotic parameter space encompassing species, height, canopy radius, disturbance, and life stage on the basis of visual distinctiveness. The matching model for a particular specimen is then obtained by simply snapping to the closest sample in the parameter space. This has the advantage that a reference atlas can be constructed off-line and applied to all simulations sharing a common biome (see Figures 14 and 15).

In our experiments, based on the Pyrenees region, we sought to reach a balance between variety and atlas complexity by using the following quantization parameters:

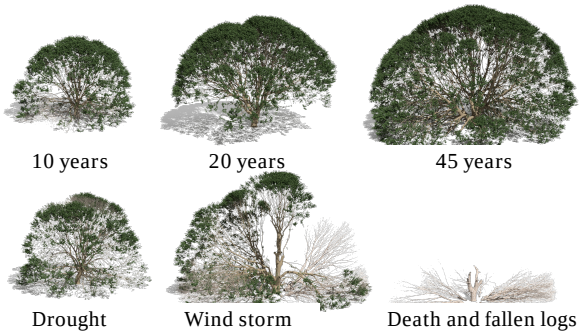

Fig. 14. Typical examples of tree geometries $\mathcal{G}$ stored in the reference atlas.

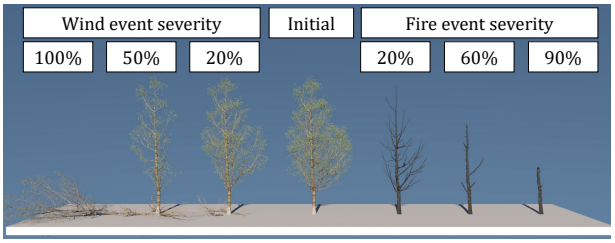

Fig. 15. Examples of wind- and fire-damaged tree geometries $\mathcal{G}$ in our reference atlas. These are sourced from the same initial tree and capture gradiations of damage according to fire and wind severity.

(1) *Species:* Seven endemic species in the region were chosen on the basis of prevalence and ecological niche, representing a mix of trees and shrubs (see Table 5).
(2) *Height:* Tree forms were selected at four different key heights for each species, capturing different development stages spanning from early shrub-like forms to apex maturity. Note that height is a better basis for quantization than age because growth and form are influenced so strongly by environmental factors. For instance, a tree that is sunlight starved in the undergrowth and consequently stunted for most of its lifespan can undergo a sudden spurt of growth due to an opening in the canopy (captured in Botany by so-called forest gap models) and this behavior is more strongly correlated with resource access than age.
(3) *Canopy Radius:* For each height two versions of the tree were instanced with minimum and maximum canopy extent, based on a life history of dense or sparse local sunlight competition.
(4) *Life Stage and Disturbance:* Since the visual impact of fire and wind disturbance and the different stages of decay is so distinctive, we decided to create separate instances for fire (3) and wind (3) damage and various levels of decay (8).

In total, this gives rise to a reference atlas with 784 unique 3D tree models (7 species × 4 heights × (6 disturbance events + 8 life stages) × 2 radii). To populate the forest floor we determine grass density and height on the basis of residual moisture and sunlight after casting canopy shade and then use this to pick suitable grass patches.

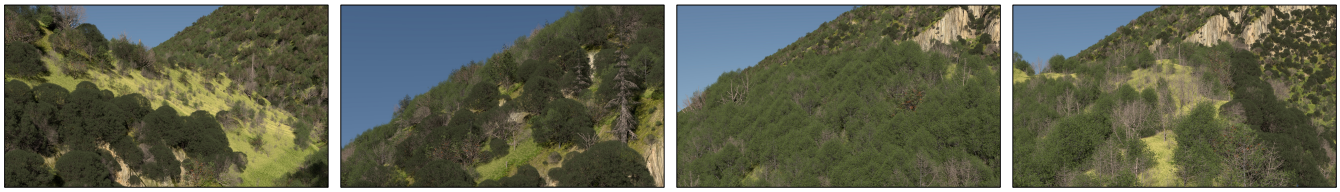

Fig. 16. Varied views of a relatively dense forest on sloping ground (2 × 2km terrain, 1.14M trees).

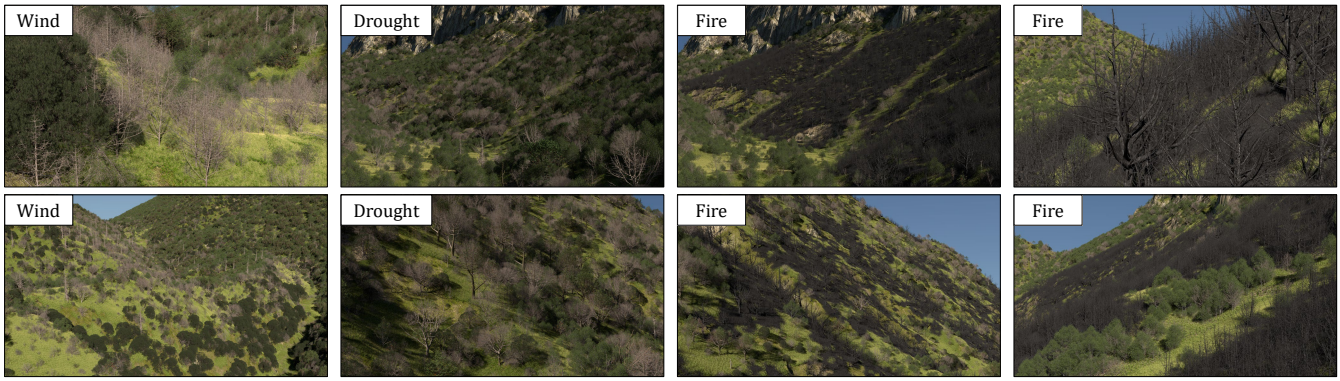

Fig. 17. Views demonstrating the visual consequences of extensive wind, drought, and fire damage.

Overall, our quantization strategy has the virtue of supporting precomputation but is not ideal in other respects. It does not adapt to the actual spread and clustering of specimens in parameter space evident in a particular simulation. Also, our choice of parametrization for large scenes does not consider the entirety of life history. For instance, only the most recent disturbance event is taken into account. However, a more nuanced parametrization combined with on-demand instance selection and matching would need an effective automated means of sampling on a perceptual basis.

In addition, the variety and realism of close-up shots is improved by adding grass, leaves, small branches and rock patches according to tree density (see Figures 11 and 20). A more complex simulation of the forest floor ecosystem and its varied grasses, forbs and fungi is left as future work.

7 RESULTS

We implemented our system in C++, with OpenGL used for previsualization. Experiments were conducted on an Apple Mackbook Pro laptop with an M1 Pro processor containing 32 GB of RAM and 8 cores (6 performance and 2 efficiency, clocked at 3.22GHz and 2.06GHz, respectively). System outputs were exported to a custom Mitsuba renderer for final photorealistic image and video generation.

We have included several examples to indicate the impact of: topography on species and density distribution (Figures 1 and 28), progressive decay on scene appearance in the middle- and far-field (Figures 16 and 20), and disturbance events, including drought, wind, and fire (Figure 17). These serve a role as illustrative examples, but the merits of our scheme are more comprehensively assessed through a perceptual study, validation, expert feedback, and performance experiments.

7.1 Perceptual study

There has been a recent trend towards automated perceptual testing of the realism of individual trees [Polasek et al. 2021] and terrain [Rajasekaran et al. 2022; Scott and Dodgson 2022], offering the prospect of faster and less costly perceptual evaluation. Unfortunately, in the ecosystem domain such techniques have not yet reached sufficient maturity. Accordingly, we undertook a two-alternative forced choice (2AFC) study with $n = 116$ participants to test the separate and combined impact of disturbance, decay and model variety on the perceived realism of computer-generated forest environments. As treatments we considered five forms of model realization applied to the same simulation:

- Base (**B**) with a single model per species;
- Variety (**V**) with 8 models per species in different growth stages evenly distributed between dense and isolated settings, but excluding snags and logs;
- Deadwood (**D**) with 8 models per species across all life states (3 live trees, 3 snags, 2 logs);
- Variety-Deadwood (**VD**) with 48 models per species covering a multiplicative combination of different growth (4), life states (6), and sparse or dense crowding (2), and
- Variety-Deadwood-Events (**VDE**), which took the **VD** model set but focused the camera on areas of recent disturbance by fire or wind.

For each of these categories we rendered 9 short videos of 4 seconds duration (see supplementary material) from viewpoints with similar characteristics in terms of depicting trees at both middle and far distances. Each video included a consistent but small scale camera

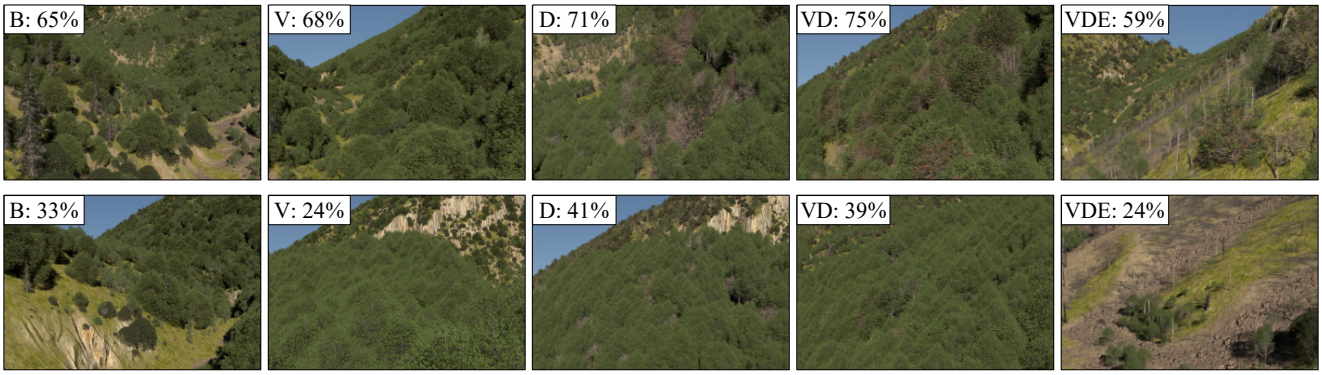

Fig. 18. Best (top) and worst (bottom) performing viewpoints for each scene type (**B** = base, **V** = variety, **D** = deadwood, **VD** = variety-deadwood, and **VDE** = variety-deadwood-events). Percentages indicate the proportion of times the image was selected as being more realistic out of the total times shown.

translation intended to improve discernment of scene depth and canopy detail.

The perceptual study was browser-based and administered over the Internet. Although we did not specify a required display resolution, we encouraged them to use a laptop or desktop monitor. In each of 22 trials a user was required to choose the more realistic (*"Which of the two scenes do you perceive as more realistic?"*) of two videos presented side-by-side in a two-alternative forced choice (2AFC) design. Care was taken to ensure that paired videos began and looped synchronously. Participants were allowed to change their selection within a trial by clicking on a video up until finally confirming their choice, but could not return to previous trials. Each evaluation consisted of 20 unique video pairs in which each of the ten possible pairings of treatments was considered twice with different videos in all cases, as well as 2 repeated control pairs. Presentation was randomized in terms of the order of trials, the video selected from among the nine possibilities for each treatment, and the left or right placement in the browser. The control pairs were included as a consistency check. If a participant changed their selection in both controls then we discarded all their trial data due to the likelihood of them having submitted random responses.

The study was advertised among hiking groups on mailing lists and social media with a view to recruiting participants with greater exposure to real rather than digital nature. After consistency checks, we obtained data from 116 participants, of whom 70% reported hiking on a regular basis (monthly or weekly), and 58% never played video games containing natural environments (see Table 3 for a more detailed demographic breakdown). We did not ask participants for their gender or age, as we did not consider this information to be influential in this study.

In terms of statistical testing, we performed a Bayesian analysis with the probability of a scene type t being chosen modeled as a Bernoulli random variable with probability θ_t. Starting from uniform Beta prior distributions, Figure 19 shows the posterior distributions obtained for θ_t. To assess statistically significant differences, we computed the credible intervals corresponding to 95% of each probability density function, as shown in the figure. Thus, if the intervals for two conditions a and b do not overlap, it is credible to infer that θ_a and θ_b have different values and the condition with larger θ is preferred.

		Gaming				
		A	**B**	**C**	**D**	Total
Hiking	**A**	1	1	0	1	3
	B	16	6	6	3	31
	C	11	8	5	1	25
	D	39	6	4	8	57
	Total	67	21	15	13	116

Table 3. Distribution of responses to demographic questions in our perceptual study pertaining to regularity of experiencing natural forests (hiking) and playing games containing simulated outdoor environments (gaming). Possible reponses were: **A**) *never or rarely* (less than once a year), **B**) *occasionally* (a few times a year), **C**) *often* (every month), or **D**) *usually* (every week or almost).

In interpreting these results, we note that the presence of deadwood (snags and logs) appears to be more crucial to perceptual realism than model variety. This is evidenced by the statistically significant preference for deadwood scenes (**D** and **VD**) over others, combined with a lack of significant preference for the inclusion of variety on its own (e.g., **D** vs. **VD**). The exception is the case of scenes dominated by disturbance events (**VDE**), which were rated worst. We regard this as anomalous and attribute it to issues with our ground textures not adequately capturing burn patterns, combined with a possible preference for more dense and verdant spaces. The most unexpected outcome was that introducing variety (**V**) to a single-instance baseline (**B**) damaged perceived realism. One possible explanation is that one model in the baseline (**B**) contained darker branches, whereas the instances in the variety case (**V**) were more uniform in color despite their variation in other respects. This points to a need to carefully design the instantiation process on a perceptual basis. In conclusion, there is evidence that the inclusion of decay processes in the simulation and rendering of natural scenes contributes to improving visual realism. To aid the interpretation of these results, Figure 18 contains images of the most and least favored scene in each treatment.

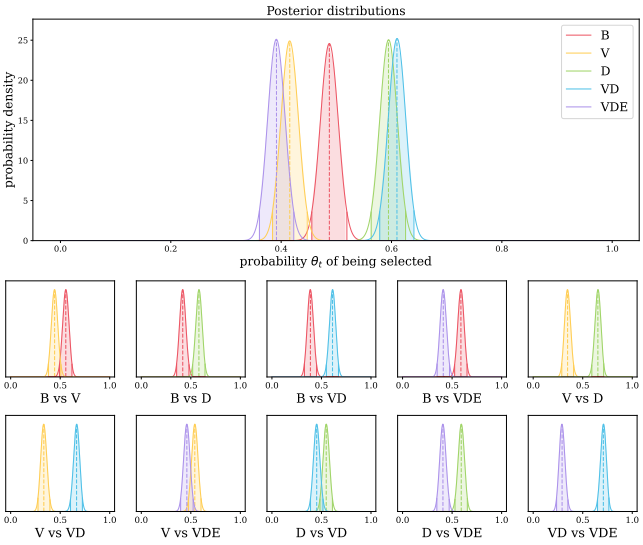

Fig. 19. Posterior beta distributions for θ_t obtained from our 2-AFC study. (Top) The combination of all pairwise distributions. (Bottom) Distribution matrices for individually paired scene types. Shaded areas represent the 95% credible interval and dashed lines the mean for θ_t.

7.2 Validation

We chose to validate our simulation model using a region in the Pyrenees mountains of northern-eastern Spain, specifically the Gresolet valley and surrounds. The area in question has a mixture of climates, including sub-Mediterranean and Euro-Siberian, as a result of local topography that spans a range of altitudes from 1200 – 1600 m. A variety of typical European tree and plant species flourish in the area, predominantly European Beech, Mountain Pine, Sessile Oak, Silver Fir and Boxwood (see Table 5). This region was chosen because it contains forests that are mature, relatively sheltered from human disturbance, varied in terms of species representation, and also well documented.

To tune and validate our model we ran an experiment over a timespan sufficient for maturity (800 years) on an area in Gresolet $2 \times 2\,\text{km}^2$ in extent containing both valleys and steep slopes. We validated the final tuned model on the following basis (see Figure 27):

(1) *Species distribution* - The distribution of species in the area generally obey the following patterns [Marmi Plana 2000]: mountain pine occurs at higher altitudes and on slopes, beech dominates in the cool, moist valleys, and oak and fir are mixed among the beech forest depending on the microclimate. These occurrence patterns are replicated in our experiments as evident in the symbolic rendering in Figure 21, which highlights the species by color.
(2) *Species basal area* - Species occupancy is often recorded using basal area, which is the sum of the cross-sectional area for all trees of a specific species and diameter threshold (7.5cm in this case), measured at breast height (≈ 1.3m) and then normalized per hectare. Given available data from a nearby parcel in Spain's National Forest Inventory [1], the expectation is that Mountain Pine, European Beach, and Silver Fir will dominate at around 16.2, 17, and 8.5 m^2/ha, respectively. We achieve similar proportions of species (equal Mountain Pine and European Beech at 12.7 and 12.3 m^2/ha, with Silver Fir half that level ($6.4m^2/ha$) at the 800 year mark) but not absolute numbers, likely due to the extensive cliffs in the area.
(3) *Succession behavior* - It is worth noting that Silver Fir serves as a pioneer species in some biomes [Volařík and Hédl 2013] and this role is confirmed by its initial dominance prior to the 150 year mark, after which it is overtaken by European Beach and later Mountain Pine.
(4) *Snag and log proportions* - The reported proportions of snags and logs in old-growth temperate forests [Nilsson et al. 2002] are as follows: Measured by basal area, snags represent approximately 10% of all standing trunks (the typical range is 8 – 12%), and 30% of the combined deadwood (range 20 – 40%). As can be seen in Figure 27, our simulation accords with these proportions once maturity is reached, with live trees at $35.8m^2/ha$, snags at $4.5m^2/ha$, and logs at $13.5m^2/ha$, representing a snag:standing proportion of 11.2% and a snag:deadwood proportion of 25%. Figure 22 demonstrates how, in the absence of disturbance, decaying trees are spread across the entire simulation domain, as is predictable for even-aged cohorts.

To validate our disturbance modules we applied a scripted scenario incorporating a mix of disease, droughts, windstorms and forest fires to the Gresolet scene setup. Unfortunately, we were not able to obtain a detailed history of disturbance events in the region so these represent an exploratory scenario. The basal area impact of these disturbances can be seen in Figure 27.

Disease. At the 250 year mark we initiated a Mountain Pine specific infectious disease, designed to emulate the pine processionary moth. This was modeled with a period $m_{\text{contagious}} = m_{\text{recover}} = m_{\text{immune}} = 12$ months, low-to-moderate vitality impact, and possible reinfection. While the basal area growth of Mountain Pines slows, there is no perceivable increase in snags and logs, as is to be expected from a disease whose main effect is defoliation rather than tree death. As demonstrated in Figures 13 and 23, after a pronounced first wave of the disease, successive waves tend to flatten and converge into a situation of endemic equilibrium, as modeled in epidemics in which Recovered individuals can become Susceptible again due to loss of immunity [Bjørnstad et al. 2020].

Windstorms. The scenario incorporates three severe windstorms powerful enough to uproot trees and split trunks: (1) 92 km/h winds from the SE at year 350; (2) 117 km/h winds from the NW at year 470, and (3) 102 km/h winds from the NE at year 590. It is worth noting that the basal area impact of these windstorms varies between species, depending on their modulus of rupture (MOR) values. A double peak in the snag and log curves is also evident, coincident with and then 5 – 10 years after the event, corresponding to the initial damage followed by secondary decay of snags and damaged trees.

[1] Parcel P_00018, obtained from https://laboratoriforestal.creaf.cat/nfi_app/

Fig. 20. A comparison of under-storey scenes without (above) and with decay, snags and logs (below). Both scenes have the same ground details, including grass, leaves and small logs.

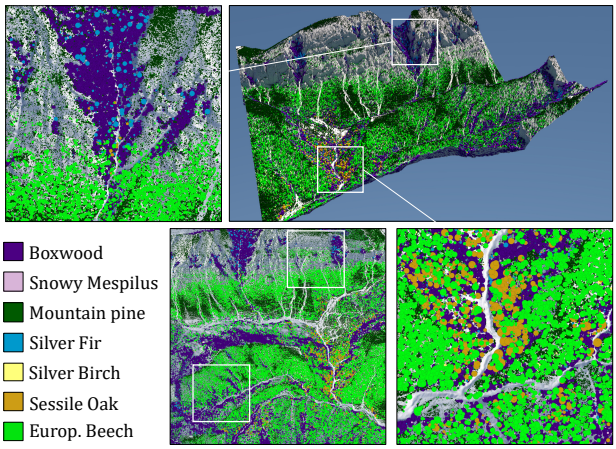

Fig. 21. A false color map showing species prevalence at year 800 of our undisturbed validation experiment. Note the prevalence of Beech and Oak in the well-watered valleys, as compared to Boxwood, Mountain Pine, and Silver Fir at higher altitudes.

Droughts. There are two periods of drought in the scenario: (1) from year 400 a yearlong dry spell with precipitation at $10-30\%$ of normal levels, and (2) from year 504 a two year spell with $20-40\%$ precipitation levels, combined with a fire in year 505. The ecosystem displays fair drought resistance, with firs and beeches being most susceptible, likely at the edges of their adaptation zone. However, the exacerbating effect of drought on fire is noteworthy.

Forest fires. In August of year 504 after 19 months of drought we simulated a wildfire event with three source locations, two of which merge into a single fire front. This wildfire burns a combined 41 ha and represents the single most damaging event in the timeline. In contrast, a subsequent fire in year 550 with similar intensity but falling outside the dry spell burns only 11 ha. Furthermore, in Figure 24 we show a side-by-side comparison of a satellite orthoimage of the Gresolet region and our computer-generated scene. Note that, although the coloring is different, particularly because Boxwood appears almost black and river areas are left bare in the CG scene, the growth patterns are roughly similar.

Instance matching vs. individual growth. Finally, we weighed the visual effect of our tree instantiation procedure against the alternative of growing every tree individually, based on its simulation history (see Figure 25). The experiment was conducted on a small 30×30m terrain, with an ecosystem comprising 166 trees and bushes of various sizes. Instantiation from our atlas took ≈ 1 second, whereas the individualized growth process required 990 seconds. In doing so, we accelerated individual tree growth by approximating the occlusion of sunlight due to surrounding trees using proxy cylinders. Simulating the local light environment with accurate tree geometry would have been even slower. For instantiation, we introduced random rotation to better hide visible cloning. Obviously, individualized growth provides better adaptation to the environment at a significant memory and computation cost, but the differences can be hard to discern if the instantiation atlas is sufficiently diverse.

We also compared the outcomes of instance matching and individualized growth after applying two sets of consecutive events to a grove (Figure 26). The overall appearance remains consistent in both cases, albeit with minor variations. Our instancing uses a rough approximation of the local light and crowding environment, whereas individualized growth is far more accurate in this respect. Furthermore, the keen observer may detect duplicated logs and tree models in the case of instantiation, although, as already mentioned, this can be ameliorated by increasing the size of the atlas.

7.3 Expert feedback

In order to more closely interrogate the realism of our generated ecosystems, we solicited feedback from 4 experts: 2 botanists and 2 CG artists, specializing in landscapes. We showed them various images and short videos of landscapes generated with our framework, both with and without the deadwood component. They provided feedback on the overall realism, with a focus on the impact of death and decay, the requirement for fine detail, and some aspects of plant distribution.

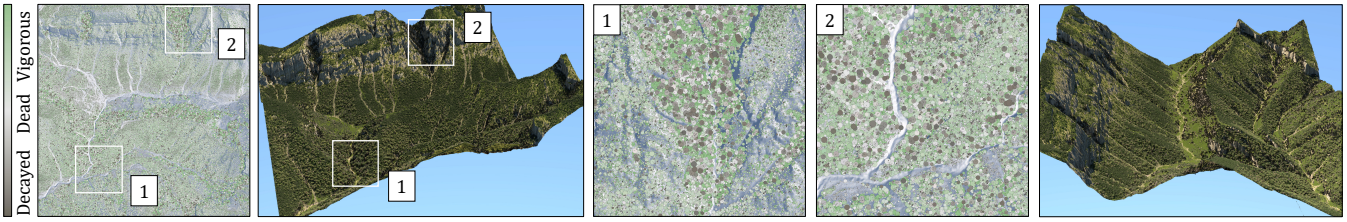

Fig. 22. Ecosystem life-state visualized using a bi-color spectrum from full vigor (green) through death (white) to full decay (black). The mature undisturbed scenario shown here exhibits the co-occurrence of trees in the full range of states.

Terrain	Number			Basal	Time		Proportion spent on		
area (km^2)	Live	Snags	Logs	area (m^2)	Year	Total	Decay	Seeding	Growth
0.5×0.5	108k	9k	10k	987	0.8s	$0.1h$	0.095	0.023	0.882
1.0×1.0	508k	38k	43k	3679	3.7s	$0.45h$	0.158	0.019	0.823
1.5×1.5	1120k	83k	94k	7462	8.9s	$1.11h$	0.248	0.017	0.735
2.0×2.0	2073k	144k	165k	11317	18.22s	$2.9h$	0.355	0.015	0.63

Table 4. Simulation performance on terrains of different extent, comparing: the average number of live trees, snags, and logs in the ecosystem; the average total un-normalized basal area of live trees per year; the average computation cost of a single simulation year in seconds; the total runtime of the simulation up to 500 years in hours, and the proportion of time spent on death and decay, seeding, and growth. Note that averages are calculated over the period from 100 to 500 years to avoid early variability.

Fig. 23. Disease onset and recovery: during the course of the disease plant vigor is impacted (visible in the loss of foliage) but over time trees recover and develop immunity.

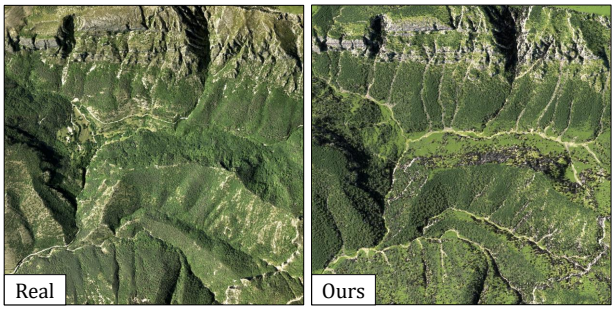

Fig. 24. A side-by-side comparison of real (left) and simulated (right) ortho-images of the Gresolet region in the Pyrenees.

Impact of death and decay. The experts confirmed that the presence of dead trees, logs and fallen branches not only significantly improved the perceived realism of generated landscapes, but also provided clues as to the health of the forest and the occurrence of disturbance events. Conversely, they felt that an absence of death and decay left the forests looking unnaturally uniform.

Geometry and texture detail. In terms of specific detail, the CG artists identified the collar where the trunk meets the ground as an area needing improvement, and reported investing significant effort in their own work to model this juncture, typically adding visible root flare and forest floor deformation. They also pointed out a lack of aging and weathering of the bark, and the absence of moss, ivy, lichen and fungus. The botanists observed the need for blossoms, flowers and fruit. They also felt that the transition between live and dead branches was too abrupt and that dead wood should have a darker shading. All experts agreed that the different species were well differentiated but sought more color variation within species.

Plant distribution. The CG artists found the overall distribution of dead trees realistic and noted the presence of clearings with coherent patterns of trees, shrubs, and saplings. From an authoring perspective, they would likely have further augmented this by including more groves and clearings. The botanists noted that different species vary in the way they break or fall, depending on the structure of their root systems, which can vary from shallow and wide (e.g., firs) to narrow and deep (e.g., oaks). Another aspect not captured is the distribution of trees on ridges, which tends to be sparse except for a few large specimens. They also felt that, with regard to the four decay states (bare, debranched, snapped, and stump, as illustrated in

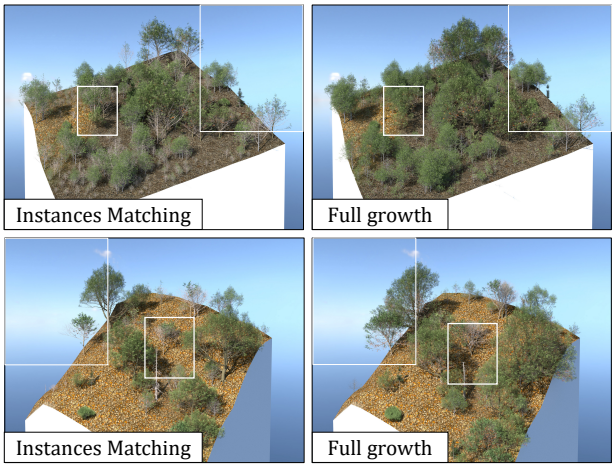

Fig. 25. A side-by-side comparison of instance matching (left) and full model realization of each individual tree (right) on a 30m × 30m landscape. The two scenes are very similar and difficult to differentiate.

Figure 9), our system over-represents the bare stage, which is relatively transitory. However, this could easily be rectified by adjusting the decay class transition. They also pointed out that dead trees provide resources to the environment and that, beyond promoting seedlings, they more favorably impact the development of small vegetation, such as ferns.

These interviews confirmed the importance of portraying death and decay, and validated our general simulation strategy. We note the many comments focused on the geometry, texture, and small details of the tree models themselves, for which we only claim a marginal contribution. This does open interesting avenues for further work, however.

7.4 Performance

Table 4 shows the performance statistics of our simulator, including execution times, for scenes of various sizes, ranging from $0.5 \times 0.5\,\mathrm{km}^2$ to $2 \times 2\,\mathrm{km}^2$, over a timespan of 500 years. This simulation timespan is sufficient for our Pyrenees test case to reach early maturity. While our simulator is capable of tracking the life history of millions of trees on large terrains, it must be acknowledged that computation times are lengthy in such cases. A uniform grid is used to accelerate neighborhood interaction tests. However, our implementation is currently CPU-based and a GPU re-implementation, to which such a grid-based approach is well suited, would likely improve runtimes substantially. As a point of performance comparison, the GPU-enabled Sylviculture system [Makowski et al. 2019] takes roughly twice as long (7.1s per year for $462\,k$ trees, at their maximum reported ecosystem size). This is only to be expected since they consider trees at a finer level of detail.

In terms of scalability, we have found that the absolute number of trees in the simulation domain for a given timestep is not a wholly accurate predictor of computation cost. While the death and decay subsystem does scale linearly with the total number of snags and logs, this is not the case for growth. A better predictor for this component is the total basal area (the sum of the basal area of all live trees in the simulation). This is because much of the growth computation involves evaluating light transmission and water absorption in canopy and root cells and cell occupancy varies with basal area. This relationship is evident in Table 4, which is based on concentric crops of the Gresolet terrain. The central region of this terrain (0.5×0.5km scale) is more favorable for growth so that trees live longer and grow larger with a higher proportion of time spent on growth. When the less favorable periphery is included at larger scales (2×2km), leading to lower basal areas, the proportion of time spent on death and decay increases.

7.5 Limitations

In terms of limitations, a user needs to be aware of the long computation times required to generate deadwood environments: up to several hours, depending on the size of the terrain and ecosystem density. Nevertheless, the decision to disentangle model realization from ecosystem simulation provides advantages in scale and computational performance over more tightly coupled simulators [Makowski et al. 2019]. It might also be possible to incorporate decay and disturbance into interactive ecosystem authoring systems [Gain et al. 2017; Kapp et al. 2020] by extending disc-based synthesis to include snags and logs.

Another weakness shared by many ecosystem simulation systems is the need to tune parameters to fit a specific biome. Our general strategy is to obtain initial values from the literature. For instance, the European Atlas of Forest Tree Species [Commission et al. 2016] provided us with approximate abiotic tolerances for species endemic to the Pyrenees. Nevertheless, subsequent fine-tuning remains essential. This is complicated by parameter sensitivity and species interactions. For instance, a relatively small change in drought tolerance might allow a species to unrealistically dominate a particular niche by outcompeting other species. This process thus requires patience and expertise.

In terms of disturbance events, we have focused on natural phenomena that include drought, disease, wind and fire. However, our approach is modular and could be readily extended to include events triggered by humans and animals [Ecormier-Nocca et al. 2021], such as grazing, forest management, and road construction.

One final limitation lies in the size and coverage of the sampling atlas. We chose a relatively uniform sampling with 784 unique trees, a choice largely dictated by memory limitations arising during instance rendering. Although this demonstrated credible differences in our perceptual study, it does introduce sampling error in that a specific tree's history and shape must be approximated by one of the instances in the atlas. The alternative for smaller scenes is to generate each tree as a unique instance (as we demonstrate in Figure 25), but this does not scale well. Another implication is that our method is better suited to generating snapshots of ecosystems at specific times rather than videos of temporal evolution. The latter would require a very dense atlas with temporally coherent models sampled at yearly intervals. Nevertheless, it would be worth exploring strategies that support larger atlases with automated perceptually-based sampling and tuning for specific use cases, such as severely damaged environments or temporal evolution. In general, a deeper

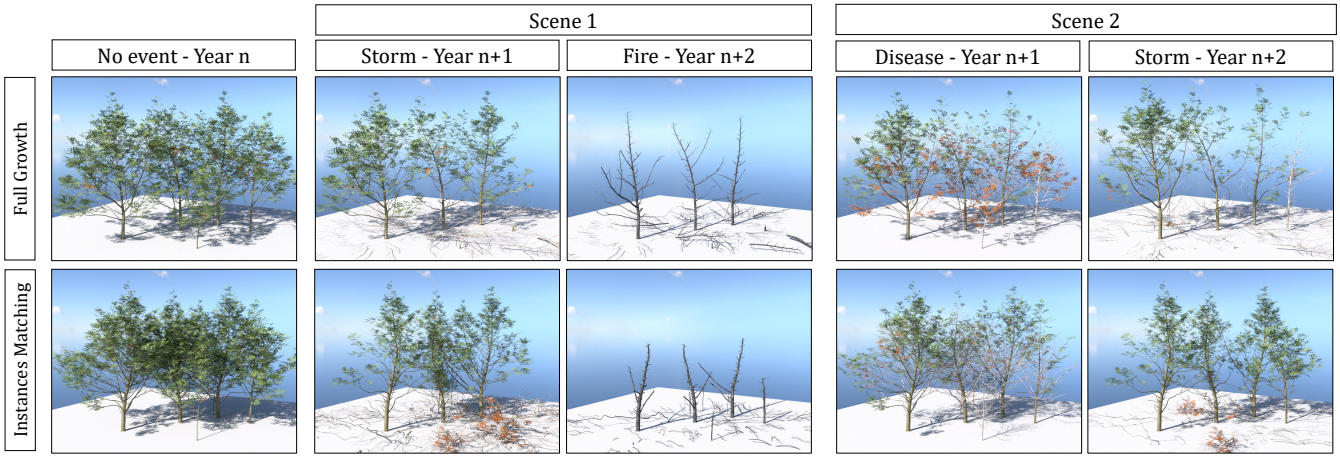

Fig. 26. A visual comparison of individual model growth (top) and instance matching (bottom) for sequences of disturbance events. This covers two distinct situations: In case 1, a storm is followed by a subsequent fire, while in case 2, a year of disease is immediately followed by a storm.

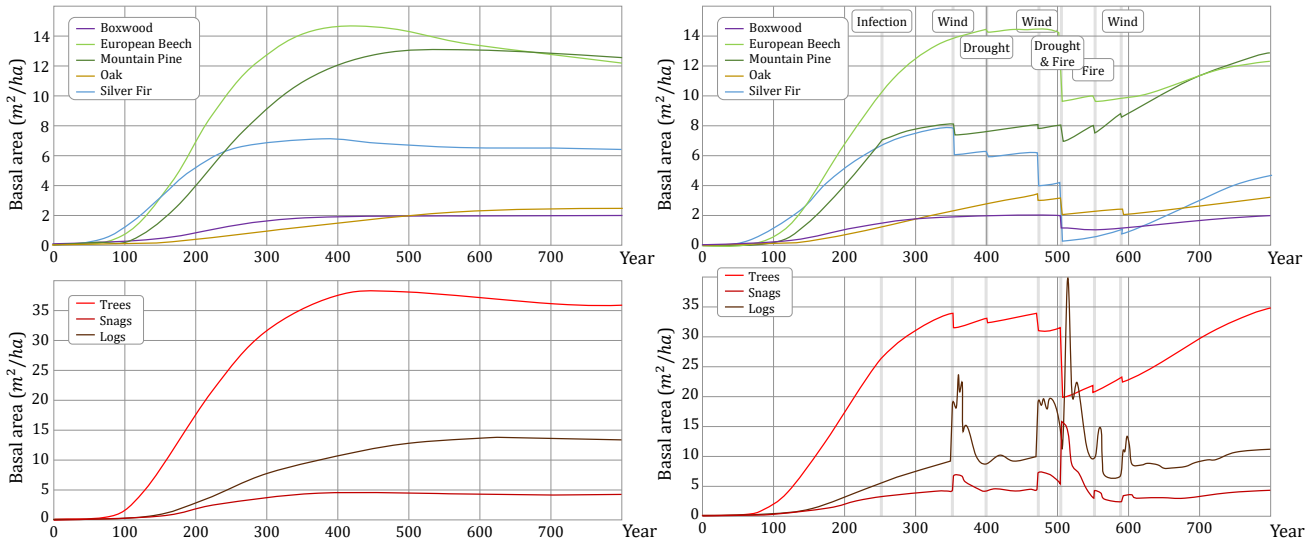

Fig. 27. Normalized basal area trajectories in two scenarios, one with no disturbance events (left column) and in a scene subject to a series of disease, drought, fire, and windstorm events, showing species (above) and life stage (below).

investigation into how to trade off memory and computation complexity, visual fidelity, and authoring control through the generation of sampling atlases is certainly warranted.

8 CONCLUSION

Plant ecosystems are impacted by a wide variety of disturbance events from human and natural sources, including, among others, diseases, droughts, windstorms and forest fires. In combination with decay processes, which transition dead trees from intact snags and logs to decomposed humus, these represent a major source of visual variety in natural environments.

Accordingly, we have presented a multi-component framework for ecosystem simulation and modelling that emphasises decay processes and disturbance events. This involves the model realization of individual tree instances through a growth process that respects life history, an enhanced large-scale ecosystem simulation that tracks the stages of sprouting, growth, disturbance, death, and decay for constituent trees, and a mechanism for matching between the simulation and model realization outputs on the basis of life history. This framework is capable of handling large scenes up to $2 \times 2\,\mathrm{km}^2$ in size containing millions of plants. We have confirmed the efficacy of our framework and the importance of deadwood processes through a perceptual study ($n = 116$), which indicates that digital scenes containing snags and logs are perceived as more realistic

	Common name	Scientific name	Form	$\hat{\ell}_s$	$\hat{\delta}_s$	$\hat{h}_s$	$\hat{\phi}_s$	q	α_s	Trnsp.	C	MOR	Wood ρ	Sun c	Sun r	Moisture c	Moisture r	Temp. c	Temp. r	Slope c	Slope r	Growth period
	Boxwood	Buxus sempervirens	Shrub/Tree	300	100	9	0.2	-5	1	0.7	162	45	600	3.75	4.25	27.5	12.5	11.75	23.25	0	80	L
	Snowy Mespilus	Amelanchier ovalis	Shrub	50	30	6	0.1	-4	1	0.52	162	45	600	7	5	31	9	19.25	15.75	0	80	S
	Mountain Pine	Pinus uncinata	Tree	400	50	20	1	-4	5	0.43	162	44	505	7	5	21.5	18.5	11.75	23.25	0	80	L
	Silver Fir	Abies alba	Tree	550	50	50	2	-6	2	0.47	145	42	415	5	3	31	9	11.75	23.25	0	80	L
	Silver Birch	Betula pendula	Tree	120	30	30	0.6	-4	30	0.3	162	63	640	8.25	3.75	27.5	12.5	19.25	15.75	0	70	S
	Sessile Oak	Quercus petraea	Tree	600	120	40	3	-7	6	0.35	162	59	710	5	3	37.5	22.5	19.25	15.75	0	70	S
	European Beech	Fagus sylvatica	Tree	400	30	50	3	-4	0.3	0.37	162	65	710	5.75	6.25	37.5	22.5	19.25	15.75	0	70	S

Table 5. A summary of species parameters used in our Pyrenees simulations, indicating symbolic rendering color; both common and scientific names; form; maximums for lifespan ($\hat{\ell}_s$), deathspan ($\hat{\delta}_s$), height ($\hat{h}_s$), and crown diameter ($\hat{\phi}_s$); height tuning (q); log seeding multiplier (α_s); crown transparency; pulling coefficient (C), modulus of rupture (MOR), and wood density (ρ). Also included are parametric responses (c, r values) for sunlight, moisture, temperature, and slope, and the growth period (S = 6 months, L = 9 months). Sources: crown transparency [Randolph et al. 2010], log seeding [Bolton and D'Amato 2011], wood density [Harmon et al. 2004], pulling and rupture [Seidl et al. 2012], and abiotic responses [Commission et al. 2016].

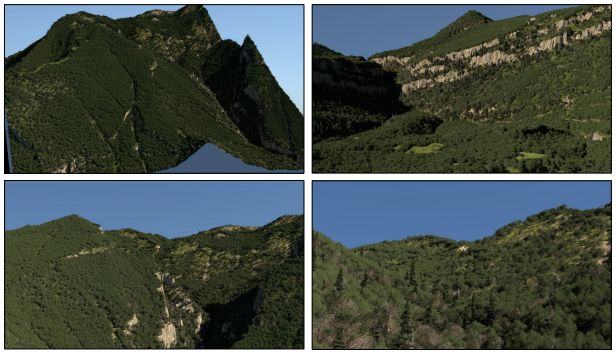

Fig. 28. A scene generated on an alternate terrain sourced from the Vimboca region in the Pyrenees. The terrain has fewer sheltered valleys and is somewhat more mountainous leading to a lower density of trees ($900k$ vs. $1340k$ on a $1.5 \times 1.5\,\mathrm{km}^2$ terrain).

than those without, and that this effect is more prominent than general specimen variation.

ACKNOWLEDGMENTS

This work was funded by the project AMPLI ANR-20-CE23-0001, supported by Agence Nationale de la Recherche (France), by the National Research Foundation of South Africa (Grant Number:129257) and is also part of a Maria Zambrano fellowship by Ministerio de Universidades (Spain).

REFERENCES

Tuomas Aakala, Timo Kuuluvainen, Sylvie Gauthier, and Louis De Grandpré. 2008. Standing dead trees and their decay-class dynamics in the northeastern boreal old-growth forests of Quebec. *Forest Ecology and Management* 255, 3 (2008), 410–420.

Alex Alexandridis, Dimitris Vakalis, Constantinos I. Siettos, and George V. Bafas. 2008. A cellular automata model for forest fire spread prediction: The case of the wildfire that swept through Spetses Island in 1990. *Appl. Math. Comput.* 204, 1 (2008), 191–201.

Monssef Alsweis and Oliver Deussen. 2005. Modeling and Visualization of symmetric and asymmetric plant competition. In *Eurographics Workshop on Natural Phenomena*, P. Poulin and E. Galin (Eds.). The Eurographics Association, 83–88.

Monssef Alsweis and Oliver Deussen. 2006. Wang-tiles for the simulation and visualization of plant competition. In *Computer Graphics International*. Springer, 1–11.

Carlos Andújar, Antonio Chica, Miguel A. Vico, Sergio Moya, and Pere Brunet. 2014. Inexpensive Reconstruction and Rendering of Realistic Roadside Landscapes. *Computer Graphics Forum* 33, 6 (2014), 101–117.

Bedrich Benes, Nathan Andrysco, and Ondrej Stava. 2009. Interactive Modeling of Virtual Ecosystems. In *Eurographics Workshop on Natural Phenomena*, Eric Galin and Jens Schneider (Eds.). Eurographics Association, 9–16.

Ottar N. Bjørnstad, Katriona Shea, Martin Krzywinski, and Naomi Altman. 2020. The SEIRS model for infectious disease dynamics. *Nature Methods* 17, 6 (2020), 557–558.

Nicholas W. Bolton and Anthony W. D'Amato. 2011. Regeneration responses to gap size and coarse woody debris within natural disturbance-based silvicultural systems in northeastern Minnesota, USA. *Forest Ecology and Management* 262, 7 (2011), 1215–1222.

Gwyneth Bradbury, Kartic Subr, Charalampos Koniaris, Kenny Mitchell, and Tim Weyrich. 2015. Guided Ecological Simulation for Artistic Editing of Plant Distributions in Natural Scenes. *Journal of Computer Graphics Techniques* 4, 4 (2015), 28–53.

Derek Bradley, Derek Nowrouzezahrai, and Paul Beardsley. 2013. Image-Based Reconstruction and Synthesis of Dense Foliage. *ACM Transactions on Graphics* 32, 4 (2013), 74:1–10.

Eugene Ch'Ng. 2013. Model resolution in complex systems simulation: Agent preferences, behavior, dynamics and n-tiered networks. *Simulation* 89, 5 (2013), 635–639.

European Commission, Joint Research Centre, T Houston Durrant, D De Rigo, A Mauri, G Caudullo, and J San-Miguel-Ayanz. 2016. *European atlas of forest tree species*. Publications Office.

Guillaume Cordonnier, Eric Galin, James Gain, Bedrich Benes, Eric Guérin, Adrien Peytavie, and Marie-Paule Cani. 2017. Authoring Landscapes by Combining Ecosystem and Terrain Erosion Simulation. *ACM Transactions on Graphics* 36, 4 (2017), 12.

Brett Desbenoit, Eric Galin, and Samir Akkouche. 2004. Simulating and modeling lichen growth. *Computer Graphics Forum* 23, 3 (2004), 341–350.

Oliver Deussen, Patrick Hanrahan, Bernd Lintermann, Radomir Měch, Matt Pharr, and Przemyslaw. Prusinkiewicz. 1998. Realistic Modeling and Rendering of Plant Ecosystems. In *Proceedings of the 25th Annual Conference on Computer Graphics and Interactive Techniques (SIGGRAPH '98)*. ACM, 275–286.

Julie Dorsey, Alan Edelman, Henrik Wann Jensen, Justin Legakis, and Hans Køhling Pedersen. 1999. Modeling and Rendering of Weathered Stone. In *Proceedings of the 26th Annual Conference on Computer Graphics and Interactive Techniques (SIGGRAPH '99)*. ACM Press/Addison-Wesley Publishing Co., 225–234.

Pierre Ecormier-Nocca, Guillaume Cordonnier, Philippe Carrez, Anne-marie Moigne, Pooran Memari, Bedrich Benes, and Marie-Paule Cani. 2021. Authoring Consistent Landscapes with Flora and Fauna. *ACM Transactions on Graphics* 40, 4 (2021), 13.

Pierre Ecormier-Nocca, Pooran Memari, James Gain, and Marie-Paule Cani. 2019. Accurate Synthesis of Multi-Class Disk Distributions. *Computer Graphics Forum* 38, 2 (2019), 157–168.

Shawn Fraver, Amy Milo, John Bradford, Anthony D'Amato, Laura Kenfic, Brian Palik, Christopher Woodall, and John Brissette. 2013. Woody Debris Volume Depletion Through Decay: Implications for Biomass and Carbon Accounting. *Ecosystems* 16 (2013), 1262–1272.

Grégoire Freschet, James Weedon, Rien Aerts, Jurgen van Hal, and Johannes Cornelissen. 2012. Interspecific differences in wood decay rates: Insights from a new short-term method to study long-term wood decomposition. *Journal of Ecology* 100 (2012), 161–170.

James Gain, Harry Long, Guillaume Cordonnier, and Marie-Paule Cani. 2017. EcoBrush: Interactive Control of Visually Consistent Large-Scale Ecosystems. *Computer*

Graphics Forum 36, 2 (2017), 63–73.

Barry A. Gardiner and Christopher P. Quine. 2000. Management of forests to reduce the risk of abiotic damage – a review with particular reference to the effects of strong winds. *Forest ecology and Management* 135, 1-3 (2000), 261–277.

Torsten Hädrich, Daniel T. Banuti, Wojtek Pałubicki, Sören Pirk, and Dominik L. Michels. 2021. Fire in Paradise: Mesoscale Simulation of Wildfires. *ACM Transactions on Graphics* 40, 4, Article 163 (2021), 15 pages.

Torsten Hadrich, Bedrich Benes, Oliver Deussen, and Sören Pirk. 2017. Interactive Modeling and Authoring of Climbing Plants. *Computer Graphics Forum* 36, 2 (2017), 49–61.

Sophie E. Hale, Barry Gardiner, Andrew Peace, Bruce Nicoll, Philip Taylor, and Stefania Pizzirani. 2015. Comparison and validation of three versions of a forest wind risk model. *Environmental Modelling & Software* 68 (2015), 27–41.

Mark Harmon, Jerry Franklin, Frederick Swanson, Phillip Sollins, Stanley Gregory, John Lattin, N. H. Anderson, Steven Cline, Nicholas Aumen, James Sedell, George G.W. Lienkaemper, Kermit Cromack, and Kenneth Cummins. 2004. Ecology of Coarse Woody Debris in Temperate Ecosystems. In *Advances in Ecological Research: Classic Papers*. Advances in Ecological Research, Vol. 34. Academic Press, 59–234.

Mathieu Henry, Antonio Bombelli, Carlo Trotta, Alfredo Alessandrini, Luca Birigazzi, Gael Sola, Ghislain Vieilledent, Philippe Santenoise, Fleur Longuetaud, Riccardo Valentini, Nicolas Picard, and Laurent Saint-Andre. 2013. GlobAllomeTree: international platform for tree allometric equations to support volume, biomass and carbon assessment. *iForest - Biogeosciences and Forestry* 6, 6 (2013), 326–330.

Konrad Kapp, James Gain, Eric Guérin, Eric Galin, and Adrien Peytavie. 2020. Data-Driven Authoring of Large-Scale Ecosystems. *ACM Transactions on Graphics* 39, 6, Article 217 (2020), 14 pages.

Joseph T. Kider, Samantha Raja, and Norman Badler. 2011. Fruit Senescence and Decay Simulation. *Computer Graphics Forum* 30, 2 (2011), 257–266.

Brendan Lane and Przemyslaw Prusinkiewicz. 2002. Generating spatial distributions for multilevel models of plant communities. In *Graphics Interface '02*. Canadian Human-Computer Communications Society, 69–80.

Bosheng Li, Jacek Kałużny, Jonathan Klein, Dominik L. Michels, Wojtek Pałubicki, Bedrich Benes, and Sören Pirk. 2021. Learning to Reconstruct Botanical Trees from Single Images. *ACM Transaction on Graphics* 40, 6, Article 231 (2021), 15 pages.

Chuan Li, Oliver Deussen, Yi-Zhe Song, Phil Willis, and Peter Hall. 2011. Modeling and Generating Moving Trees from Video. *ACM Transactions on Graphics* 30, 6 (2011), 1–12.

Jiaqi Li, Xiaoyan Gu, Xinchin Li, Junzhong Tan, and Jiangfeng She. 2018. Procedural Generation of Large-Scale Forests Using a Graph-Based Neutral Landscape Model. *ISPRS International Journal of Geo-Information* 7, 3 (2018), 127–142.

Yanchao Liu, Jianwei Guo, Bedrich Benes, Oliver Deussen, Xiaopeng Zhang, and Hui Huang. 2021. TreePartNet: Neural Decomposition of Point Clouds for 3D Tree Reconstruction. *ACM Transactions on Graphics* 40, 6, Article 232 (2021), 16 pages.

Milosz Makowski, Torsten Hädrich, Jan Scheffczyk, Dominik Michels, Sören Pirk, and Wojtek Pałubicki. 2019. Synthetic Silviculture: Multi-Scale Modeling of Plant Ecosystems. *ACM Transactions on Graphics* 38, 4 (2019), 131:1–14.

Nicolas Maréchal, Eric Guérin, Eric Galin, and Samir Akkouche. 2010. Component-Based Model Synthesis for Low Polygonal Models. In *Proceedings of Graphics Interface*. ACM, 217–224.

Josep M. Marmi Plana. 2000. El bosc de Gresolet. *L'Erol: revista cultural del Berguedà* 65 (2000), 22–25.

Stéphane Mérillou and Djamchid Ghazanfarpour. 2008. A Survey of Aging and Weathering Phenomena in Computer Graphics. *Computer & Graphics* 32, 2 (2008), 159–174.

Radomir Měch and Przemyslaw Prusinkiewicz. 1996. Visual Models of Plants Interacting with Their Environment. In *Proceedings of the 23rd Annual Conference on Computer Graphics and Interactive Techniques (SIGGRAPH '96)*. ACM, 397–410.

Till Niese, Sören Pirk, Matthias Albrecht, Bedrich Benes, and Oliver Deussen. 2022. Procedural Urban Forestry. *ACM Transactions on Graphics* 41, 2, Article 20 (2022), 18 pages.

Sven Nilsson, Mats Niklasson, Jonas Hedin, Gillis Aronsson, Jerzy Gutowski, Per Linder, Hakan Ljungberg, Grzegorz Mikusiński, and Thomas Ranius. 2002. Densities of large living and dead trees in old-growth temperate and boreal forests. *Forest Ecology and Management* 161 (2002), 189–204.

Wojciech Palubicki, Kipp Horel, Steven Longay, Adam Runions, Brendan Lane, Radomír Měch, and Przemyslaw Prusinkiewicz. 2009. Self-Organizing Tree Models for Image Synthesis. *ACM Transactions on Graphics* 28, 3, Article 58 (2009), 10 pages.

Wojtek Palubicki, Miłosz Makowski, Weronika Gajda, Torsten Hädrich, Dominik Michels, and Sören Pirk. 2022. Ecoclimates: Climate-Response Modeling of Vegetation. *ACM Transactions on Graphics* 41, 4, Article 155 (2022), 19 pages.

Sören Pirk, MichałJarząbek, Torsten Hädrich, Dominik L. Michels, and Wojciech Palubicki. 2017. Interactive Wood Combustion for Botanical Tree Models. *ACM Transactions on Graphics* 36, 6, Article 197 (2017), 12 pages.

Sören Pirk, Till Niese, Oliver Deussen, and Boris Neubert. 2012a. Capturing and Animating the Morphogenesis of Polygonal Tree Models. *ACM Transactions on Graphics* 31, 6, Article 169 (2012), 10 pages.

Sören Pirk, Till Niese, Torsten Hädrich, Bedrich Benes, and Oliver Deussen. 2014. Windy Trees: Computing Stress Response for Developmental Tree Models. *ACM Transactions on Graphics* 33, 6, Article 204 (2014), 11 pages.

Sören Pirk, Ondrej Stava, Julian Kratt, Michel Abdul Massih Said, Boris Neubert, Radomír Měch, Bedrich Benes, and Oliver Deussen. 2012b. Plastic Trees: Interactive Self-adapting Botanical Tree Models. *ACM Transactions on Graphics* 31, 4, Article 50 (2012), 10 pages.

Tomas Polasek, David Hrusa, Bedrich Benes, and Martin Čadík. 2021. ICTree: Automatic Perceptual Metrics for Tree Models. *ACM Transactions in Graphics* 40, 6, Article 230 (2021), 15 pages.

Hans Pretzsch, Peter Biber, Enno Uhl, Jens Dahlhausen, Thomas Rotzer, Juan Caldentey, Takayoshi Koike, Tran van Con, Aurélia Chavanne, Thomas Seifert, Ben du Toit, Craig Farnden, and Stephan Pauleit. 2015. Crown size and growing space requirement of common tree species in urban centres, parks, and forests. *Urban Forestry and Urban Greening* 14, 3 (2015), 466–479.

Przemyslaw Prusinkiewicz, Lars Mündermann, Radoslaw Karwowski, and Brendan Lane. 2001. The Use of Positional Information in the Modeling of Plants. In *Proceedings of the 28th Annual Conference on Computer Graphics and Interactive Techniques (SIGGRAPH '01)*. ACM, 289–300.

Drew W. Purves, Jeremy W. Lichstein, and Stephen W. Pacala. 2007. Crown Plasticity and Competition for Canopy Space: A New Spatially Implicit Model Parameterized for 250 North American Tree Species. *PLOS ONE* 2, 9 (2007), 1–11.

Suren Deepak Rajasekaran, Hao Kang, Martin Čadík, Eric Galin, Eric Guérin, Adrien Peytavie, Pavel Slavík, and Bedrich Benes. 2022. PTRM: Perceived Terrain Realism Metric. *ACM Transactions on Applied Perception* 19, 2, Article 6 (2022), 22 pages.

KaDonna Randolph, Sally Campbell, and Glen Christensen. 2010. *Descriptive statistics of tree crown condition in California, Oregon, and Washington.* Technical Report. Southern Research Station, USDA Forest Service.

Tobias Ritschel, Thorsten Grosch, and Hans-Peter Seidel. 2009. Approximating Dynamic Global Illumination in Image Space. In *Proceedings of the 2009 Symposium on Interactive 3D Graphics and Games (I3D '09)*. Association for Computing Machinery, 75–82.

Matthew B. Russell, Shawn Fraver, Tuomas Aakala, Jeffrey H. Gove, Christopher W. Woodall, Anthony W. D'Amato, and Mark J. Ducey. 2015. Quantifying carbon stores and decomposition in dead wood: A review. *Forest Ecology and Management* 350 (2015), 107–128.

Hisashi Sato, Akihiko Itoh, and Takashi Kohyama. 2007. SEIB–DGVM: A new Dynamic Global Vegetation Model using a spatially explicit individual-based approach. *Ecological Modelling* 200, 3-4 (2007), 279–307.

Joshua J Scott and Neil A Dodgson. 2022. Evaluating Realism in Example-Based Terrain Synthesis. *ACM Transactions on Applied Perceptions* 19, 3 (2022), 1–18.

Rupert Seidl, Werner Rammer, and Kristina Blennow. 2014. Simulating wind disturbance impacts on forest landscapes: Tree-level heterogeneity matters. *Environmental Modelling & Software* 51 (2014), 1–11.

Rupert Seidl, Werner Rammer, Robert Scheller, and Thomas Spies. 2012. An individual-based process model to simulate landscape-scale forest ecosystem dynamics. *Ecological Modelling* 231 (2012), 87–100.

Stephan Sitch, C. Huntingford, N. Gedney, P. Levy, M. Lomas, S. L. Piao, R. Betts, P. Ciais, Pierre Cox, Pierre Friedlingstein, C. D. Jones, I. Prentice, and F. Woodward. 2008. Evaluation of the terrestrial carbon cycle, future plant geography and climate-carbon cycle feedbacks using five Dynamic Global Vegetation Models (DGVMs). *Global Change Biology* 14, 9 (2008), 2015–2039.

Juliana Tolles and ThaiBinh Luong. 2020. Modeling Epidemics With Compartmental Models. *Journal of the American Medical Association* 323, 24 (2020), 2515–2516.

An Tsoularis and James Wallace. 2002. Analysis of logistic growth models. *Mathematical Biosciences* 179, 1 (2002), 21–55.

Daniel Volařík and Radim Hédl. 2013. Expansion to abandoned agricultural land forms an integral part of Silver fir dynamics. *Forest Ecology and Management* 292 (2013), 39–48.

Jamie Wither, Frédéric Boudon, Marie-Paule Cani, and Christophe Godin. 2009. Structure from silhouettes: a new paradigm for fast sketch-based design of trees. *Computer Graphics Forum* 28, 2 (2009), 541–550.

Christopher W. Woodall and Vicente J. Monleon. 2008. *Sampling protocol, estimation, and analysis procedures for the down woody materials indicator of the FIA program.* Technical Report NRS-22. U.S. Department of Agriculture, Forest Service.

Ke Xie, Feilong Yan, Andrei Sharf, Oliver Deussen, Hui Huang, and Baoquan Chen. 2016. Tree Modeling with Real Tree-Parts Examples. *IEEE Transactions on Visualization and Computer Graphics* 22, 12 (2016), 2608–2618.

Jürgen Zell, Gerald Kändler, and Marc Hanewinkel. 2009. Predicting constant decay rates of coarse woody debris – A meta-analysis approach with a mixed model. *Ecological Modelling* 220, 7 (2009), 904–912.

Jian Zhang, Changbo Wang, Chen Li, and Hong Qin. 2019. Example-based rapid generation of vegetation on terrain via CNN-based distribution learning. *The Visual Computer* 35, 6 (2019), 1181–1191.